Journal of Structural Geology 33 (2011) 292–311

Contents lists available at ScienceDirect

Journal of Structural Geology

journal homepage: www.elsevier.com/locate/jsg

The internal geometry of salt structures – A first look using 3D seismic data from the Zechstein of the Netherlands

Heijn Van Gent [a,*], Janos L. Urai [a], Martin de Keijzer [b]

[a] Structural Geology, Tectonics and Geomechanics, Geological Institute, RWTH Aachen University, Lochnerstraße 4-20, D- 52056, Aachen, Germany
[b] Nederlandse Aardolie Maatschappij b.v. (N.A.M.), Postbus 28000, 9400 HH, Assen, The Netherlands

ARTICLE INFO

Article history:
Received 14 January 2010
Received in revised form
18 June 2010
Accepted 11 July 2010
Available online 16 July 2010

Keywords:
Zechstein
Salt tectonics
3D reflection seismic
Folding
Boudinage

ABSTRACT

We present a first look at the large-scale, complexly folded and faulted internal structure of Zechstein salt bodies in NW Europe using 3D reflection seismic reflection data from two surveys on the Groningen High and the Cleaver Bank High. We focus on a relatively brittle, folded and boudinaged, claystone–carbonate–anhydrite layer (the Z3 stringer) enclosed in ductile salt. A first classification of the structures is presented and compared with observations from salt mines and analogue and numerical models.

Z3 stringers not only are reservoirs for hydrocarbons but can also present a serious drilling problem in some areas. Results of this study could provide the basis for better prediction of zones of drilling problems. More generally, the techniques presented here can be used to predict the internal structure of salt bodies, to estimate the geometry of economic deposits of all kinds and locate zones suitable for storage caverns.

Structures observed include an extensive network of zones with increased thickness of the stringer. These we infer to have formed by early diagenesis, karstification, gravitational sliding and associated local sedimentation. Later, this template was deformed into large-scale folds and boudins during salt tectonics. Salt flow was rarely plane strain, producing complex fold and boudin geometries. Deformation was further complicated by the stronger zones of increased thickness, which led to strongly non-cylindrical structures. We present some indications that the thicker zones also influence the locations of later suprasalt structures, suggesting a feedback between the early internal evolution of this salt giant and later salt tectonics.

This study opens the possibility to study the internal structure of the Zechstein and other salt giants in 3D using this technique, exposing a previously poorly known structure which is comparable in size and complexity to the internal parts of some orogens.

1. Introduction

The sedimentary basins of NW Europe are classic areas of salt tectonics (Fulda, 1928; Richter-Bernburg, 1953a; Ziegler, 1982; Taylor, 1998; Mohr et al., 2005; Geluk, 2007; Geluk et al., 2007; Hübscher et al., 2007). The Dutch part of the Central European Basin contains five evaporite cycles of the Late Permian Zechstein Group (Z1–Z5, see: Fulda, 1928; Ziegler, 1982; Best, 1989; Taylor, 1998; Geluk, 2000; De Mulder et al., 2003; TNO-NITG, 2004; Wong et al., 2007), including a relatively brittle layer consisting of anhydrite, carbonate and clay (the "Z3 stringers"[1]).

1.1. On the importance of stringers

A large part of the world's hydrocarbon reserve is associated with evaporitic deposits (Warren, 2006), for example, in the Central European Basin, the Caspian Sea, the Gulf of Mexico, offshore Brazil, and the basins of the Middle East. Prediction of the thickness, porosity, geometry and fluid fill of stringers is of significant economic importance. In some settings in Europe as well as in Oman, stringers enclosed in the salt are hydrocarbon reservoirs (Mattes and Conway Morris, 1990; Geluk, 1997, 2000; Peters et al., 2003; Al-Siyabi, 2005; Reuning et al., 2009; Schoenherr et al., 2009a,b). Better understanding stringers in NW Europe can help the interpretation of the complex geometry and history of the hydrocarbon-bearing stringers in the Ara Salt in Oman.

In addition, in most cases the Z3 stringer is considered a drilling hazard by operators in the Central European Basin. The Carbonate Member of Z3 stringer can be significantly overpressured, with

* Corresponding author. Tel.: +49 241 80 98441; fax: +49 241 80 92358.
E-mail address: h.vangent@ged.rwth-aachen.de (H. Van Gent).

[1] The terms raft and floater are sometimes used to specify layered, competent inclusions in salt. The names raft and floater imply buoyancy, but carbonate, dolomite and anhydrite have a higher density than halite and are expected to sink under the influence of gravity over geological timescales.

0191-8141/$ – see front matter © 2010 Elsevier Ltd. All rights reserved.
doi:10.1016/j.jsg.2010.07.005

pressures up to lithostatic (Williamson et al., 1997). Overpressures in stringers are difficult to predict, therefore when planning the well path, stringers are avoided where possible and not drilled when strongly folded and/or faulted. Zechstein salt is also used for different kinds of geological storage or solution mining (Hofrichter, 1974; Coelewij et al., 1978; Bornemann, 1991; Fokker et al., 1995; Geluk et al., 2000; Van Eijs and Breunse, 2003; Evans and Chadwick, 2009) and prediction of internal structure is of major relevance in these fields (see Bornemann, 1991; Koyi, 2001; Chemia et al., 2008).

1.2. Internal and external salt tectonics

In the literature, salt structures are typically shown in two strikingly different ways. In studies using 3D seismic and well data that focus on the subsalt or suprasalt sediments and are typically hydrocarbon-related, the evaporites are invariably shown as structureless bodies (for example: Jackson and Vendeville, 1994; Jackson, 1995; Scheck et al., 2003; Mohr et al., 2005; Maystrenko et al., 2006).

On the other hand, studies of the internal structure of salt are typically salt-mining or storage-related and are based on observations from mine galleries and borehole data (for example: Krische, 1928; Richter-Bernburg, 1953a; Siemeister, 1969; Hofrichter, 1974; Richter-Bernburg, 1980; Jackson, 1985; Richter-Bernburg, 1987; Bornemann, 1991; Smith, 1996; Behlau and Mingerzahn, 2001; Schléder et al., 2008). These studies show the extremely complex internal geometry with less attention to the structure of the surrounding sediments.

Detailed observations of salt mines and drill holes (with cm-to-m resolution) display a variety of deformation structures in the salt on a wide range of scales (Krische, 1928; Richter-Bernburg, 1953a; Lotze, 1957; Borchert and Muir, 1964; Kupfer, 1968; Muehlberger, 1968; Richter-Bernburg, 1980; Schwerdtner and Van Kranendonk, 1984; Richter-Bernburg, 1987; Talbot and Jackson, 1987; Best, 1989; Jackson et al., 1990; Bornemann, 1991; Zirngast, 1991, 1996; Geluk, 1995; Burliga, 1996; Smith, 1996; Behlau and Mingerzahn, 2001; Siemann and Ellendorff, 2001; Schléder et al., 2008). Observations (typically 2D to 3D in salt mines and 1D in storage or solution mining) include boudins and folds together with shear zones (Bornemann, 1991; Geluk, 1995, 2000; Burliga, 1996; Taylor, 1998; Behlau and Mingerzahn, 2001). The folds have curved, open-to-isoclinal fold axes, and boudins from millimeter (Schléder et al., 2008) to kilometer scale (Burliga, 1996) are common. Cross-sections through the Zechstein in the Gorleben and Morsleben salt domes (Bornemann, 1991; Behlau and Mingerzahn, 2001) show isoclinal folding of the Z3. Richter-Bernburg (1980) further describes several examples of fold structures with amplitudes over half the height of the salt structures.

Field studies, from Iran and Oman, have also shown the internal complexities of surface-piercing salt domes, such as the distribution of different age salt, the position and internal deformation of solid inclusions, the microstructures and, by inference, the deformation mechanisms (among others: Jackson et al., 1990; Talbot and Aftabi, 2004; Talbot, 2008; Reuning et al., 2009; Schoenherr et al., 2009a,b; Desbois et al., 2010).

Numerical as well as analogue centrifuge and extrusion models of salt tectonics tend to assume relatively homogeneous rheological properties (although mechanical stratigraphy is used), and consequently produce relatively simple salt structures (for example: Jackson and Talbot, 1989; Van Keken et al., 1993; Koyi, 2001; Schultz-Ela and Walsh, 2002; Talbot and Aftabi, 2004; Chemia et al., 2008). It must be noted, however, that most of these models do provide a way to study structural evolution due to deforming meshes or the use of multicoloured analogue materials. Despite the relatively simple rheological models, analogue and numerical models with mechanical stratigraphy have shown the complex deformation associated with (brittle) inclusions in deforming ductile media (see, for example: Escher and Kuenen, 1929; Koyi, 2001; Goscombe and Passchier, 2003; Goscombe et al., 2004; Zulauf and Zulauf, 2005; Chemia et al., 2008; Zulauf et al., 2009; Schmid et al., 2009).

1.3. Aim of this work

In this paper we aim to contribute to the understanding of the structural style and geometry of the Z3 stringer, by describing detailed interpretations of two 3D reflection seismic surveys from the Dutch onshore and offshore. We focus on thickness variations and structural style at the scale of 30 m–20 km, to draw inferences about sedimentary and diagenetic evolution and salt tectonic processes.

2. The stratigraphy of the Zechstein

In the Dutch subsurface, the Zechstein can be subdivided in a marine lower part (Z1–Z3) and a playa-type upper part (Z4 and Z5) with more clastic deposits (Geluk, 1997, 2000). Z1–Z3 follow the classic carbonate–evaporite cycle: claystone–carbonate–gypsum–halite–potassium and magnesium salts consecutively (Warren, 2006; Geluk, 2000). The cycles correspond to major transgressions from the Arctic and evaporation of seawater in the arid Southern Permian Basin (Figs. 1 and 2, Taylor, 1998). In the northern Netherlands deposition was relatively continuous, but the sedimentary sequence has major periods of non-deposition in the south (TNO-NITG, 2004; Geluk, 2007, see also Fig. 1).

Z1 halite is absent in both areas studied in this paper (Taylor, 1998; Wong et al., 2007). The Z2 Main Dolomite member and Z2 Basal Anhydrite Member (Stassfurt Formation) are deposited directly on top of the Z1 anhydrite in both study areas. Therefore, up to the top of Z2 anhydrite, all rocks are brittle and coupled to the Rotliegend and underlying basement. The top Z2 anhydrite reflector is therefore used in this study to define top of mechanical basement (Figs. 3 and 4). The Z2 halite reaches a primary thickness between 500 and 600 m in both study areas, which was later strongly modified by salt tectonics (Taylor, 1998; Geluk, 2007; Geluk et al., 2007). Near the top of Z2 locally (not in the study areas) thick deposits of potassium–magnesium salt layers are found (Geluk, 2007). The Z3 Leine Formation starts with an approximately 1 m thick grey shale (Grey Salt Clay) with a high Gamma Ray signal in wire line logs (Taylor, 1998). The overlying Platy Dolomite ("Plattendolomit") reaches thicknesses of 30 m (Smith, 1995) to 75–90 m (Taylor, 1998) on the shelf, considerably more than in the basin where it reduces to a few meters (Taylor, 1998). On top of the Platy Dolomite the Main Anhydrite ("Hauptanhydrit") is found (Taylor, 1998; Siemann and Ellendorff, 2001). In the Dutch part of the basin the thickness of the Main Anhydrite increases from 3 m on the shelf to 45 m in the basin, with local excursions to 100 m and complex changes in thickness (Rijks Geologische Dienst, 1991, 1993, 1995; Taylor, 1998; TNO, 1998; Geluk, 2000). Local variations in the Z3 anhydrite thickness were first described by Fulda (1928) and were subsequently interpreted to result from a type of gypsum diapirism or sedimentary swells, although some were interpreted to be tectonic in nature (Langbein, 1987; Williams-Stroud and Paul, 1997; Bäuerle et al., 2000).

The Z3 Leine halite is overlain by two thick potassium–magnesium salt layers, with bischofite, kieserite, carnallite and sylvite (Coelewij et al., 1978). Primary thickness of the Z3 halite

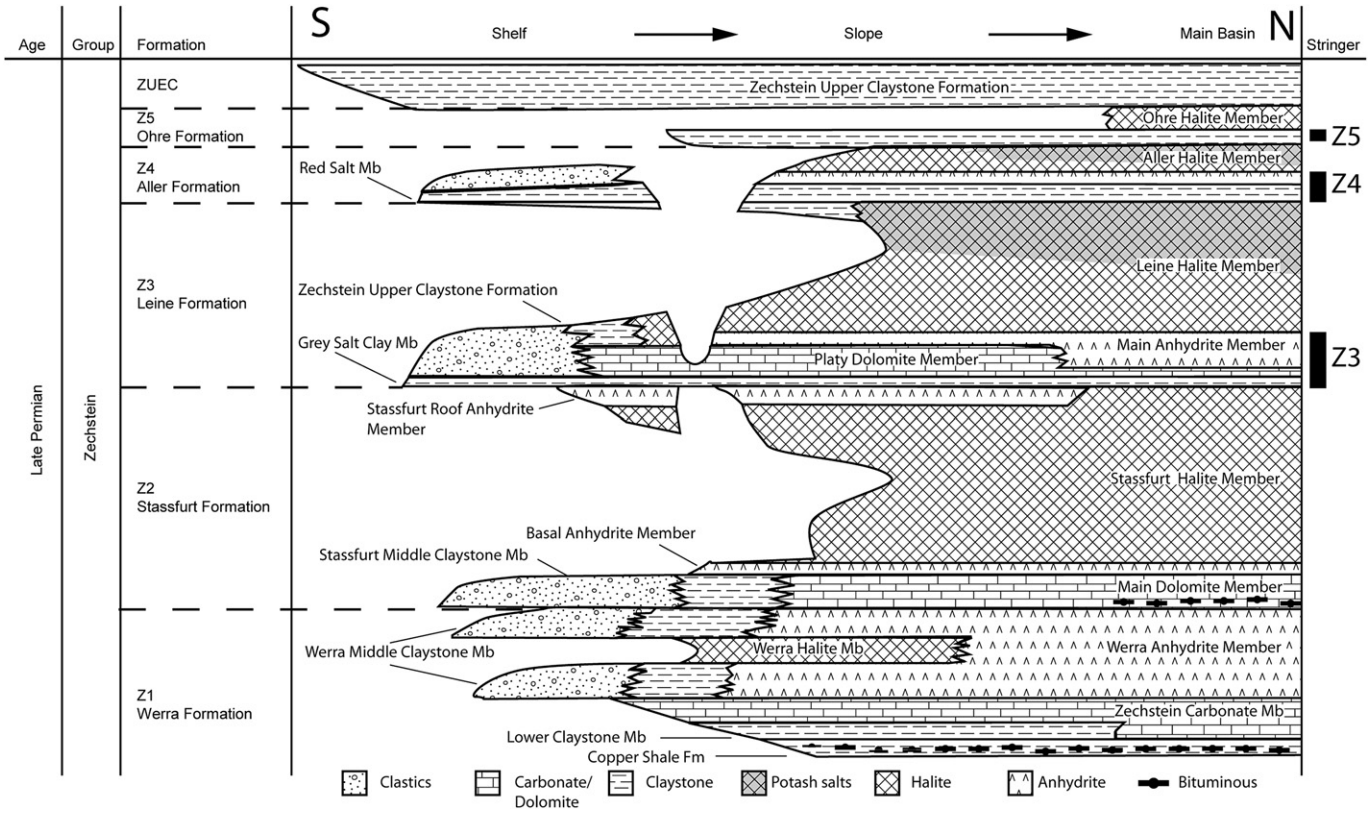

Fig. 1. Zechstein stratigraphy in the Netherlands (based on Van Adrichem-Boogaert and Kouwe, 1993–1997, Geluk, 2000 and TNO-NITG, 2004). In the right column the position of the three brittle intervals in the evaporites is indicated. Only the Z3 stringer is visible in seismic reflection data and is fully encased in halite.

is 200–300 m in the Groningen and about 100 m in the offshore study area (Wong et al., 2007).

The Aller (Z4) and Ohre (Z5) formations consist of sabkha deposits and are quite thin (Geluk, 2007). The Z6 and Z7 (Best, 1989) are not found in the Netherlands. The youngest Zechstein unit is the Upper Claystone Formation (ZUEC) which is between 10 and 50 m thick and is present in large portions of the Dutch subsurface (Van Adrichem-Boogaert and Kouwe, 1993–1997; TNO-NITG, 2004; Geluk, 2007).

2.1. The Zechstein carbonate facies (Z1–Z3)

Zechstein carbonates in the Netherlands are subdivided in shelf, slope and basin facies (Taylor, 1998; Geluk, 2000; Wong et al., 2007, see also Fig. 1). The platform carbonates consist of shallow water deposits with occasional karst features (Scholle et al., 1993; Southwood and Hill, 1995; Strohmenger et al., 1996). The carbonate members are thickest in the slope, where individual reefs and off-platform highs as well as gravity flows are found (Geluk, 2000). The basin facies was deposited in water depths up to 200 m and can contain high Total Organic Carbon (Geluk, 2000).

2.2. Z3 stringers in seismic data

The high acoustic impedance contrast between the stringer and surrounding halite makes the Z3 stringer image reasonably well in seismic data (Figs. 1 and 3). The stringer is visible as a pair of parallel loops in the relatively transparent halite. Imaging limitations are related to the frequency content and noise level of the seismic data, to the thickness of the layer and to the local high dip of the layer (Sleep and Fujita, 1997). If the thickness of the stringer is below the tuning thickness of about 30–35 m, exact thickness determination from seismic data is not possible (and thickness will be overestimated). Sections of the stringer with thicknesses below ca. 10 m are not resolved. However, the majority of stringers in the study area are typically 40–50 m thick, with local excursions up to 150 m or more (see below). The internal structure of the stringer generally is not resolved, probably because of the low impedance contrast between anhydrite and carbonate.

3. Study areas and methodology

We studied stringers in two areas: the Groningen High and the Cleaver Bank High (Fig. 2).

3.1. The Groningen High

The first study area is 20 × 30 km and is located on the Groningen High (NE Dutch onshore, Fig. 2, Van Gent et al., 2009). The Groningen Gas Field (Fig. 2) contains one of the largest gas reservoirs of the world (Stäuble and Milius, 1970; Wong et al., 2007). Mohr et al. (2005) showed that salt tectonics in the nearby Ems Graben initiated during the Early Triassic with subsequent phases in the Late Triassic and the Upper Cretaceous/Lower Tertiary. There was little or no activity between the Jurassic to Lower Cretaceous. The stringer is clearly visible in the seismic volume (Fig. 3). The data from this area is part of a large, merged, 3D pre-stack depth migrated seismic dataset, provided by the Nederlandse Aardolie Maatschappij BV. (NAM, a Shell operated 50–50 joint venture with ExxonMobil.) The horizontal resolution and seismic positioning uncertainty are around 50–75 m, with the seismic bin size being

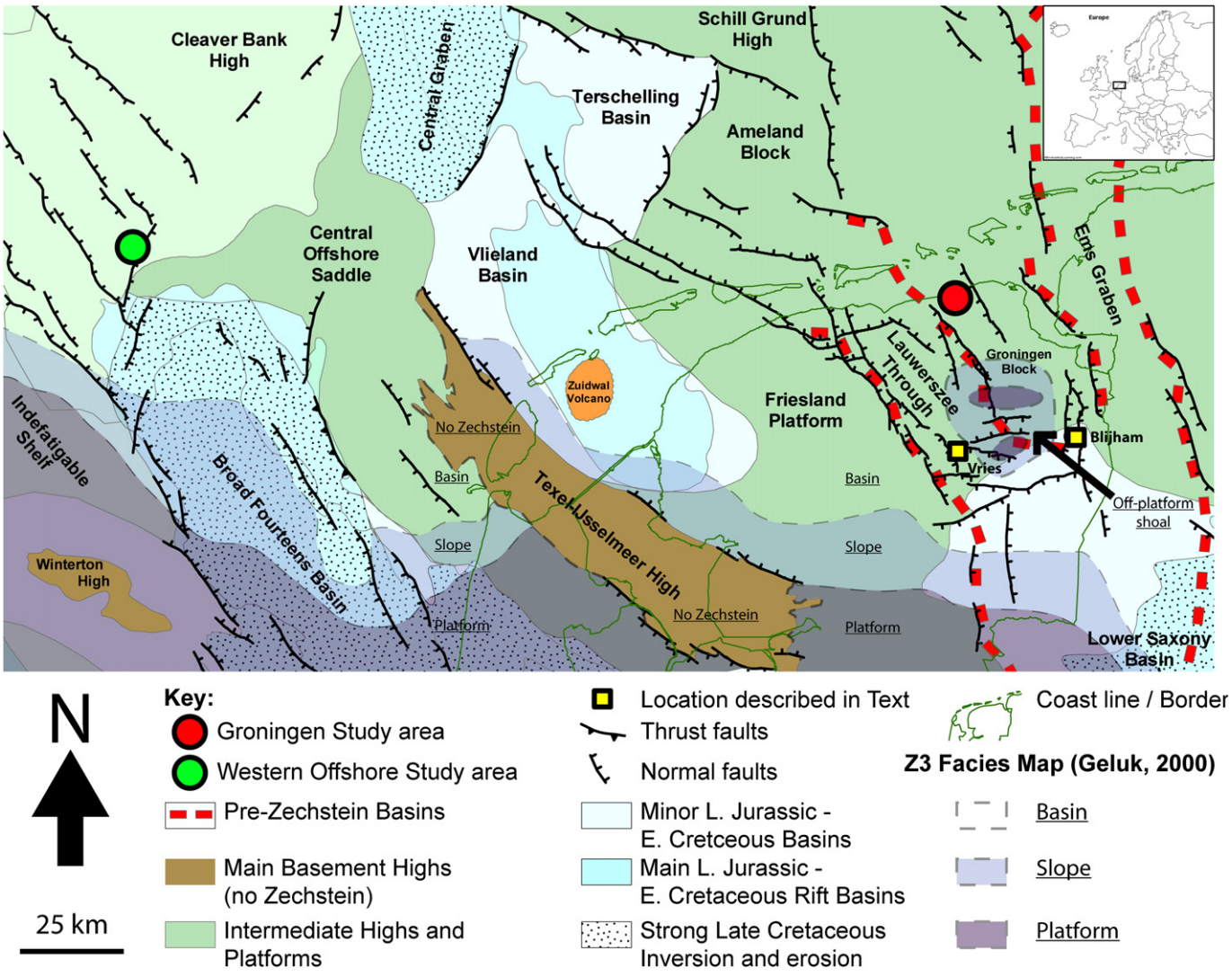

Fig. 2. Location map of the study areas with the structural elements (image courtesy of Nederlandse Aardolie Maatschappij) and Z3 paleogeography (after Geluk, 2000). On the Texel–IJselmeer High and the Winterton High no salt is present. The NW-Groningen High study area is indicated with a red dot and the offshore study area with a green dot. Locations discussed in the text are indicated with yellow dots. (For interpretation of the references to colour in this figure legend, the reader is referred to the web version of this article.)

25 m. Vertical sampling is 2–4 ms. In total over 250 wells were drilled in the Groningen area.

3.2. The western offshore

The second study area, a 20 × 20 km survey, is located in the Dutch offshore (Fig. 2), on the Cleaver Bank High (CBH), directly north of the Broad Fourteens basin, and is in close proximity to the Sole Pit Basin and the Central Graben. During the Late Carboniferous, Saalian tectonic phase, the CBH was tectonically active and uplifted. Between the Permian and the Middle Jurassic the CBH was quiet, but during the Late Jurassic to Early Cretaceous the CBH was uplifted and deeply eroded (Ziegler, 1982; Van der Molen, 2004; Duin et al., 2006). However, the study area is located outside the most important zone of erosion (Fig. 2, Van Hoorn, 1987; Van Wijhe, 1987; De Jager, 2003; Wong et al., 2007).

Top Zechstein is dominated by an NNE striking salt wall with minor grabens on both sides in the suprasalt deposits. The salt wall has a listric fault and asymmetric graben above its crest (Fig. 7, cf. Remmelts, 1996). The subsalt top Rotliegend horizon shows three fault trends (Fig. 8). The first, NW striking trend is associated with Variscan wrench faulting (Ziegler, 1982). The second, NNE trend, is parallel to the salt structure and may be related to the Central Graben/Broad Fourteens Basin fault system (see Fig. 2). The third trend is a minor, approximately E–W fault system, which is related to the northern border of the Broad Fourteens basin.

Depth and thickness maps of the suprasalt deposits show that the faults parallel to the NW trend clearly influenced the younger deposits (cf. Figs. 8 and 9).

The seismic data used for this area were also provided by NAM. The horizontal resolution and seismic positioning uncertainty are typically around 50–75 m (as the seismic bin size is 25 m). Vertical sampling is 2–4 ms. Well control is provided by a dozen production and exploration wells.

3.3. The workflow

In addition to the interpretation of the Z3 stringer, subsalt and suprasalt reflectors and major faults were used to establish a geological framework. We used the seismic interpretation package Petrel 2005 and Petrel 2007 (Schlumberger).

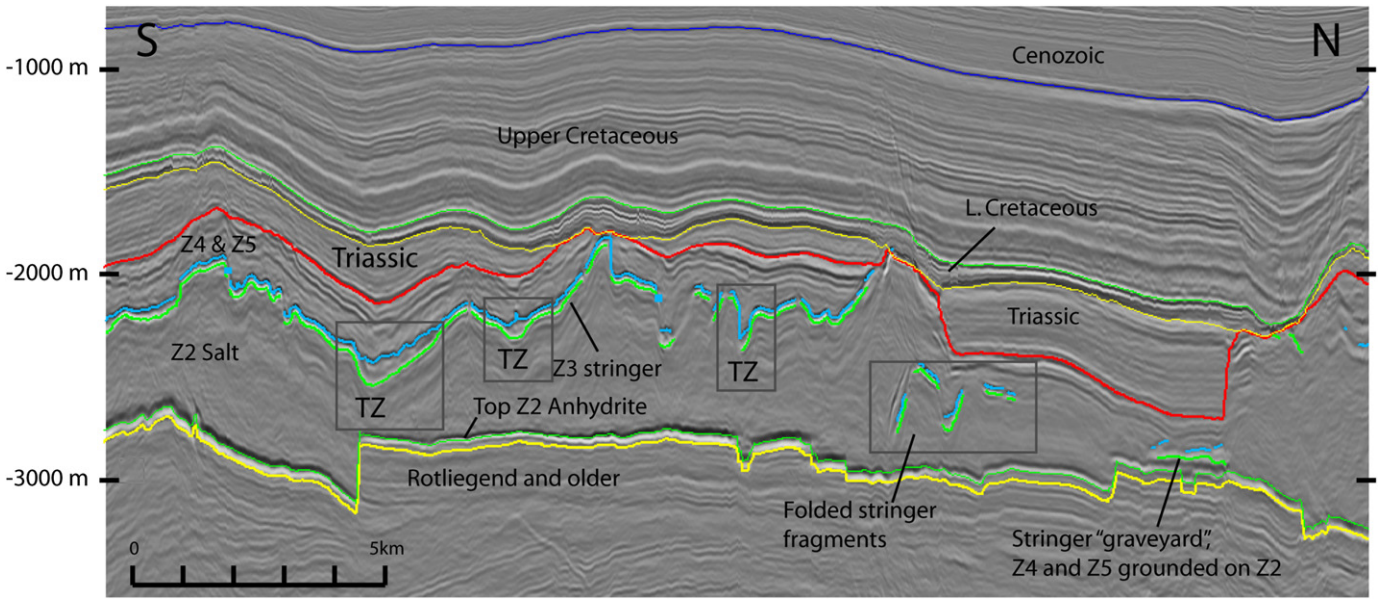

Fig. 3. N–S seismic cross-sections trough the Groningen area. The main formation bounding reflectors are indicated, as well as the top and base Z3 stringer. The Z3 stringer is relatively continuous here, although breaks in the reflector are observed. Also note the roughly 500–700 m of Z2 halite below the Z3 stringer (chaotic, weak reflectors), while above the stringer a few tens to 200 m of Z3 halite are observed between stringer and top Zechstein. The continuous, parallel reflectors directly below top Zechstein are the Playa-type deposits of the Z4 cycles. Thicker zones are indicated with TZ.

Starting from an existing interpretation (Joris Steenbrink, personal communication, 2007) in the Groningen area, the complex geometry of the stringers was studied by detailed manual interpretation. The stringers were interpreted on a 100 × 100 m seed grid, followed by seeded autotracking with a very low level of tolerance. This means in practice that the interpretation software only extends the manual interpretation a few lines away from the seed. In Groningen the Z3 stringer can be mapped with high confidence (Fig. 3). The occurrence of overlapping stringers in the offshore area (Fig. 7) provides a challenge when interpreting horizons because of the limitation of a single *z*-value at any *x*–y location in the interpretation software.

In both areas the stringer is locally less clearly defined or absent: either only one loop is visible or there is no reflector visible at all. A stringer was only interpreted in locations where both loops were visible. In the surface-building interpolation step this resulted in two continuous and overlapping surfaces in the areas without a reflector. In the Groningen area, we used the imaging resolution to define a threshold value (5 m) for the distance between these surfaces to locate "holes" in the stringer (Figs. 4d and 5a). The exact value of this threshold is not critical because the transition from seismically visible stringer to zones without visible stringer is abrupt. These holes correspond closely to the areas without well-defined stringer reflectors in cross-section (compare, for example, Figs. 3 and 4d, as well as Fig. 5).

In the offshore area we completed two different interpretations of the stringers. First, stringers were interpreted as a horizon, with very low tolerance autotracking around the manual picks. Here we consistently chose the higher stringer in case of overlap. A continuous surface was thus created over gaps in the interpretation.

In addition, we manually interpreted stringers using the "Fault Interpretation" routine of Petrel in cross-sections, at 100–200 m spacing to define a point cloud of 54 000 points. Although no realistic surface can be created in the interpretation software from these data points, this allowed interpretation of overlapping and near-vertical parts of the visible stringers and was used to study more complex 3D structures (see Section 4.3).

4. Stringer geometry

4.1. Groningen

The Base Zechstein map (top Z2 anhydrite, Fig. 4a) shows a number of basement faults with offsets up to 300 m, while the top Zechstein map (Fig. 4b) shows a few salt pillows flanked by a graben and a central area where top Zechstein is relatively horizontal at 2000–2200 m. Thickness of Zechstein is about 1000 m, increasing up to 2000 m in the salt pillows.

Although the original stratigraphic position of the Z3 stringer is about 200–300 m below top Zechstein, in its present geometry (Figs. 3, 4d, 5 and 6) its position varies from very close to top Zechstein, to very close to top Z2 anhydrite. In the central area (away from the salt pillows) the enveloping surface of the stringer is sub-horizontal and approximately in its original stratigraphic position (Fig. 4c). In what follows, we focus on areas with anomalously thick stringers, on areas where stringers are not visible, and on folds of different wavelengths, orientation and amplitudes (Figs. 3, 5 and 6).

4.1.1. Stringer thickness distribution

The observed stringers usually have a rather constant thickness of around 40 m, with areas of increased thickness (up to 150 m). We call these TZs (Thicker Zones; Fig. 3). A stringer thickness distribution map is shown in Figs. 4d and 5a (areas with no visible stringers – as defined above – are in grey).

We studied seven wells that penetrate the visible Zechstein stringer. In those wells that penetrate a TZ, the stringers are 80–125 m thick with two strong Gamma Ray peaks: one in the basal claystone and a second peak at the top. In all wells penetrating seismically visible stringers outside the TZ, stringer thickness is around 50 m with only one GR peak in the basal claystone.

In the stringer thickness map (Fig. 4d), a clearly defined regional network of up to 400 m wide, long, branching TZ is seen throughout the area (red and yellow colours in Figs. 4d and 5a, dark grey in Fig. 4e and f). These zones are curved and are connected at triple (rarely

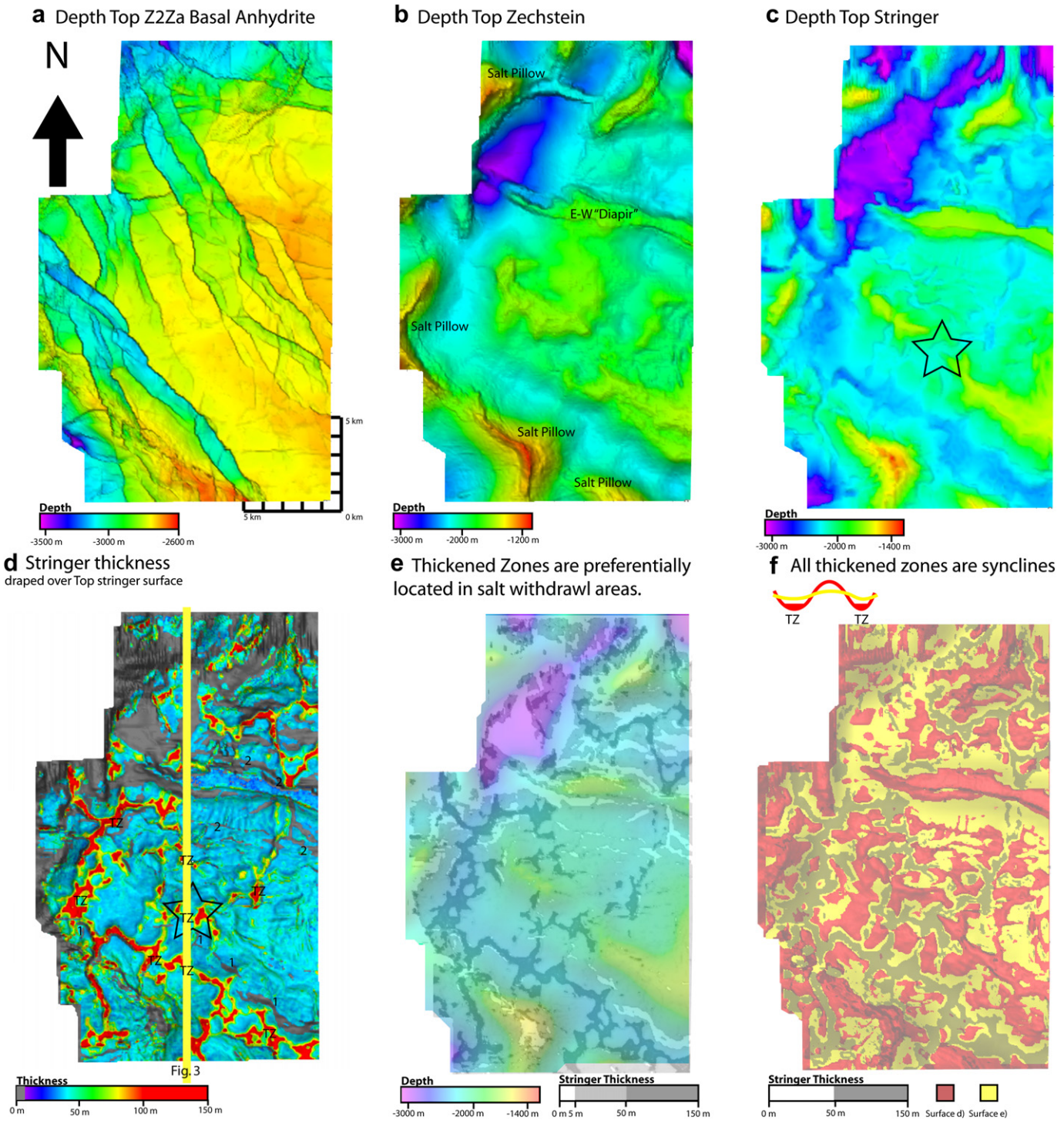

Fig. 4. a) Depth top Z2 anhydrite map, which assumed here to be the top of the mechanical basement. (b) Depth top Zechstein map. Note the structures indicated. (c) Depth top stringer map. Star denotes location where a large-scale harmonic fold is disturbed by a TZ (see Section 4.3.3. for description). (d) Thickness of the Zechstein Z3 stringer, draped over the obliquely lit top stringer surface. Note the variations in thickness and the distribution of the grey areas where the stringer is less than 5 m thick (and assumed to be absent). (e) Smoothed top stringer depth map, with a discrete stringer thickness map draped over it. Dark grey means stringer is thicker than 50 m, grey is between 5 and 50 m and white is thinner than 5 m (assumed to be absent). Note that the thicker zones always lie in the large-scale synclinal (deeper) sections of the stringer. (f) Comparison of the detailed geometry of the top stringer depth map (c, red) and the smoothed depth map (e, yellow) and the thicker sections (above 50 m). Note that the stringer is always thicker in those areas where the original depth map lies below the smoothed surface – i.e. the TZs are dominantly found in local synclinal structures. The inset shows in cross-section how the overlapping of the original (red) and smoothed (yellow) surface indicates that TZs only occur in synclines. (For interpretation of the references to colour in this figure legend, the reader is referred to the web version of this article.)

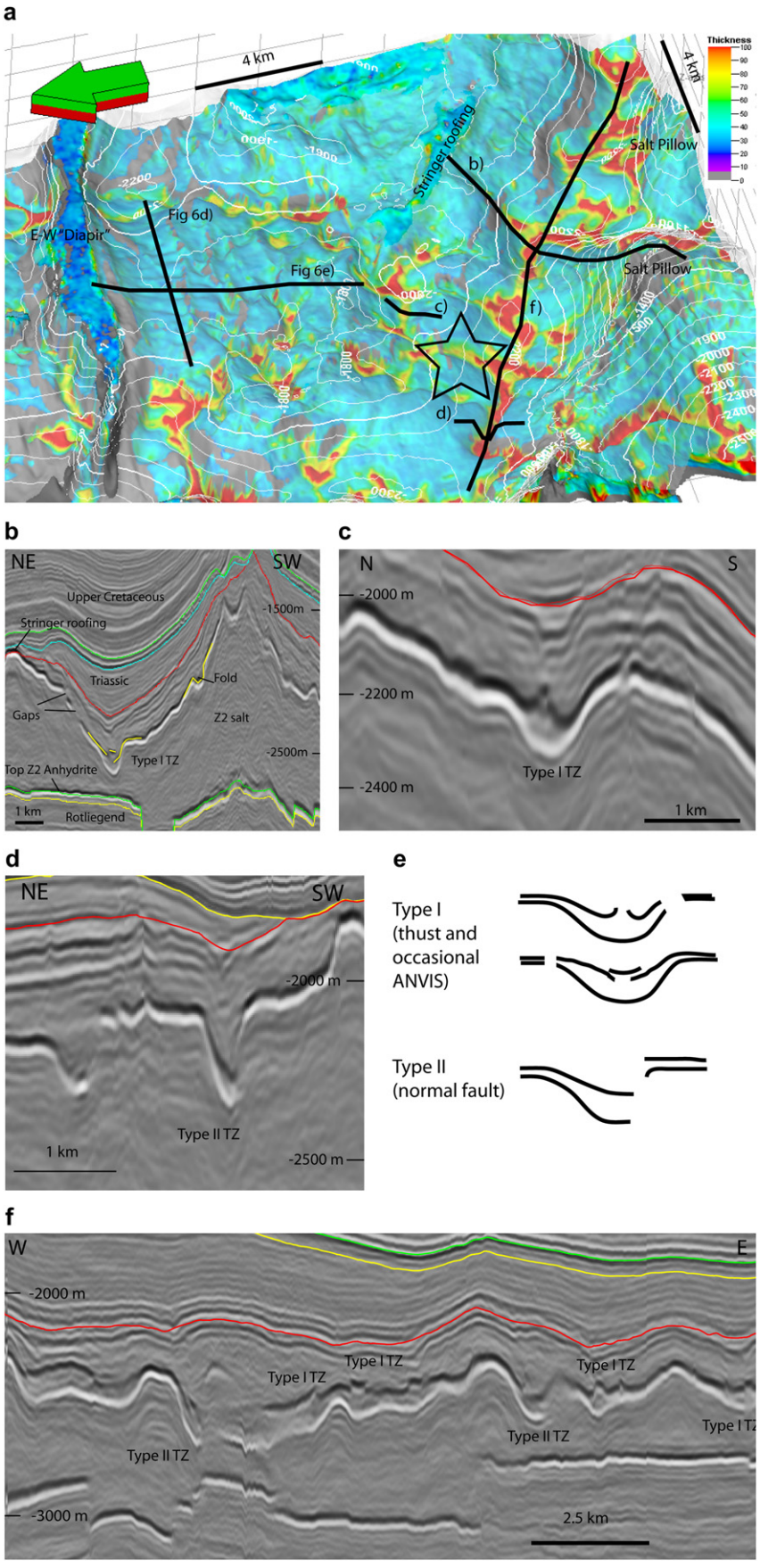
a
4 km
4 km
Thickness
Stringer roofing
b)
Salt Pillow
Fig 6d)
E-W "Diapir"
Fig 6e)
Salt Pillow
c)
f)
d)
b
NE
SW
Upper Cretaceous
Stringer roofing
-1500m
Triassic
Fold
Gaps
Z2 salt
Type I TZ
-2500m
Top Z2 Anhydrite
1 km
Rotliegend
c
N
S
-2000 m
-2200 m
-2400 m
Type I TZ
1 km
d
NE
SW
-2000 m
Type II TZ
1 km
-2500 m
e
Type I
(thust and
occasional
ANVIS)
Type II
(normal fault)
f
W
E
-2000 m
Type I TZ
Type I TZ
Type I TZ
Type II TZ
Type I TZ
Type II TZ
-3000 m
2.5 km

quadruple) junctions. TZs are synclinal (never anticlinal) in shape and lie below the stringers' enveloping surface (Figs. 4e and f and 5).

In more detail, in cross-section, TZ can be (I) symmetric, with two overlapping top stringer reflectors (top Main Anhydrite) and top stringer slightly raised in the thickest section (Figs. 5a–c and e and 6c) and a continuous base (Fig. 5a–c and e), or (II) asymmetric, with the stringer invisible on one side of the TZ (Fig. 5d–f). In the Type I TZs, structures that appear to be internal thrusts are interpreted (Fig. 5c), but it cannot be ruled out that this is an imaging effect.

There is at best a weak correlation between Rotliegend faults and TZ. In the south of the study area TZ is only roughly parallel to the Rotliegend fault trend, while the NE–SW oriented TZ along the western edge of the survey is perpendicular to this trend (compare Fig. 4a and d). There is, however, a clear correlation between TZ and the topography of top Zechstein (compare Fig. 4b and e), as well as in local depressions of the stringer (Fig. 4e and f): TZs are dominantly found in areas where top Zechstein is deep.

4.1.2. Folds

The enveloping surface of ZE3 forms 10 km-scale fold structures which are harmonic with the top Zechstein (Figs. 3 and 4). TZs are located in the synclinal hinges of these large-scale folds. In the area marked with a star in Figs. 4c and d and 5 (also visible in Fig. 6a), a TZ crosses an anticlinal structure. Here the amplitude of the anticline is much lower than in the rest of the fold.

On a smaller (km) scale, fold structures also exist, most clearly expressed in areas away from TZ. The seismic section in Fig. 6d is parallel to the E–W diapir (see Figs. 5 and 6b). A number of low wavelength (200 m) folds are observed in the stringer, while the Z2, Z4 and Z5 are not folded in the same way. Since the latter are mechanically coupled to the basement and top salt, respectively, this suggests that the folding of the Z3 solely results from movements in the salt. These folds have fold axes perpendicular to the axis of the diapir (Fig. 6b). Fig. 6c shows a similar structure of folds in an area with fold axes running up the crest of a salt pillow and wavelengths of a few 100 m. The observed fold axes in Figs. 4–6 generally are in the dip direction of the Z3 enveloping surface.

4.1.3. Areas with no visible stringer

Areas with No Visible Stringer reflector – called ANVIS – are common in the Groningen study area. In some cases, TZ is spatially related to ANVIS in sub-parallel, occasionally en-echelon, zones (ANVIS, key 1 in Fig. 4d and also Fig. 5a). In other areas, ANVIS have no apparent relationship with TZ but are related to the E–W striking salt diapir in the north of the area (key 2 in Fig. 4d). These ANVIS are clearly elongated and sub-parallel to the axis of the diapir on its southern side, most clearly expressed where no TZ is present. On the northern side of the diapir ANVIS are also present but here the presence of TZs do not allow a clear attribution to TZ or the diapir. The cross-section in Fig. 6e cuts through these gaps showing a series of asymmetric monoclines with lengths between 250 and 1000 m. The Z4 and Z5 reflectors in this area do not show the same structure, suggesting once again that the Z3 salts serve as a decoupling layer.

In four wells penetrating ANVIS, two wells encountered no stringer. In one case a very thin (10–20 m) stringer was encountered. Finally, one well in an ANVIS penetrated a 100-m long, steeply dipping stringer section, this shows that the stringers' visibility can be limited by their dip.

In the east of the survey, the roughly N–S oriented TZ intersects the E–W diapir (Figs. 4d and 6d). Here the ANVIS which are sub-parallel to the diapir crest further west curve towards the diapir and the diapir is also narrower here. This may suggest that TZs are older than ANVIS.

4.2. Western Dutch offshore

Compared to the Groningen area, the Z3 stringer in the offshore study area has a much more complex structure. In seismic cross-sections (Fig. 7, indicated in Fig. 8d) the visible Z3 stringer is less continuous and varies strongly in depth over short distances. The stringer is more intensely folded and frequently offset vertically over more than half of the total Zechstein thickness. The Mesozoic tectonic inversion of the Broad Fourteens basin is manifested in several inverted basement blocks in the area (Fig. 7).

The individual interpreted stringer fragments in this area are relatively chaotic, with a weak trend of their long axis parallel to the axis of the salt wall in the east (Fig. 8c and d). Additional trends are recognized, for example, the alignment of stringer fragments along the NW trend of basement faults in the NW of the study area (Fig. 8) and along the NW–SE trending faults in the overburden (Fig. 9).

The stringer surface which was created by horizon interpretation, autotracking and surface interpolation, is, as expected, quite similar to the point cloud interpretation which was created using the fault interpretation routine (in areas with no overlapping stringers – compare Figs. 8c and 10). The point cloud, however, shows locally a high level of additional complexity (Fig. 11). TZs were not observed in this survey; where the stringer could be interpreted, the top and bottom reflectors were about 40 m apart. ANVIS occurred in a larger fraction of the area than in Groningen.

At the regional scale, top Rotliegend shows several inverted blocks (Fig. 8a) and top Zechstein shows the NE–SW striking salt wall with two secondary, NW–SE striking graben structures which are all clearly associated with fault systems in the overburden (Figs. 8b and 9). On average the stringer is several hundreds of meters higher on the west side of the salt wall than on the east side. The Z3 stringer is very close to the top of the inverted basement blocks in almost every case studied (see also Figs. 7 and 11).

4.2.1. Stringer surface geometry

The base stringer is shown in Figs. 8e and 10. There are a number of clearly defined structural elements. Firstly, the enveloping surface of the stringers follows the large-scale salt wall (Figs. 7a and 8b). In the areas where the stringers can be autotracked and dip less than 30° (areas with bright colours and grey dots in Fig. 10) the surface shows gentle, open folds (F in Figs. 7 and 8e) with a wavelength of around 400 m and amplitude less than 200 m. Fold axes are usually curved and do not show a clear preferred orientation. Second, the surface is frequently offset (O in Fig. 8, see also Fig. 12) along steep (steeper than 35°, grey in Fig. 10 and steeper than 45°, grey in Fig. 12) discontinuities. This offset can be more or less symmetric (graben like, G in Figs. 8 and 12) or monoclinal (M in Fig. 12). The offsets can be not only small and become zero towards

Fig. 5. (a) Observations of the Z3 stringer in the Groningen area, based on a shaded oblique view of the top stringer (arrow points north, green is up, red is down). The stringer thickness (Fig. 4d) is projected on the surface, with thickness less than 10 m is grey. Also shown is the top Zechstein (white contours) and locations of cross-sections shown in b–f as well as those in Fig. 6. Vertical exaggeration is 2×. Star is in the same location as in Fig. 4. Note how the TZs in all cross-sections are always in a syncline (Fig. 4f). (b) Cross-section of internal thrusts (Type I), gaps and folds in a cross-section through the TZ. Note that the TZ is located where the stringer is low. Reflectors have the same colours in the following cross-sections. (c) Close-up cross-section of an internal thrust in the stringer (Type I). (d) Cross-section of Type II TZ. (e) Conceptual sketch of Type I and Type II TZ. (f) Cross-section showing Types I and II TZs in the same profile. (For interpretation of the references to colour in this figure legend, the reader is referred to the web version of this article.)

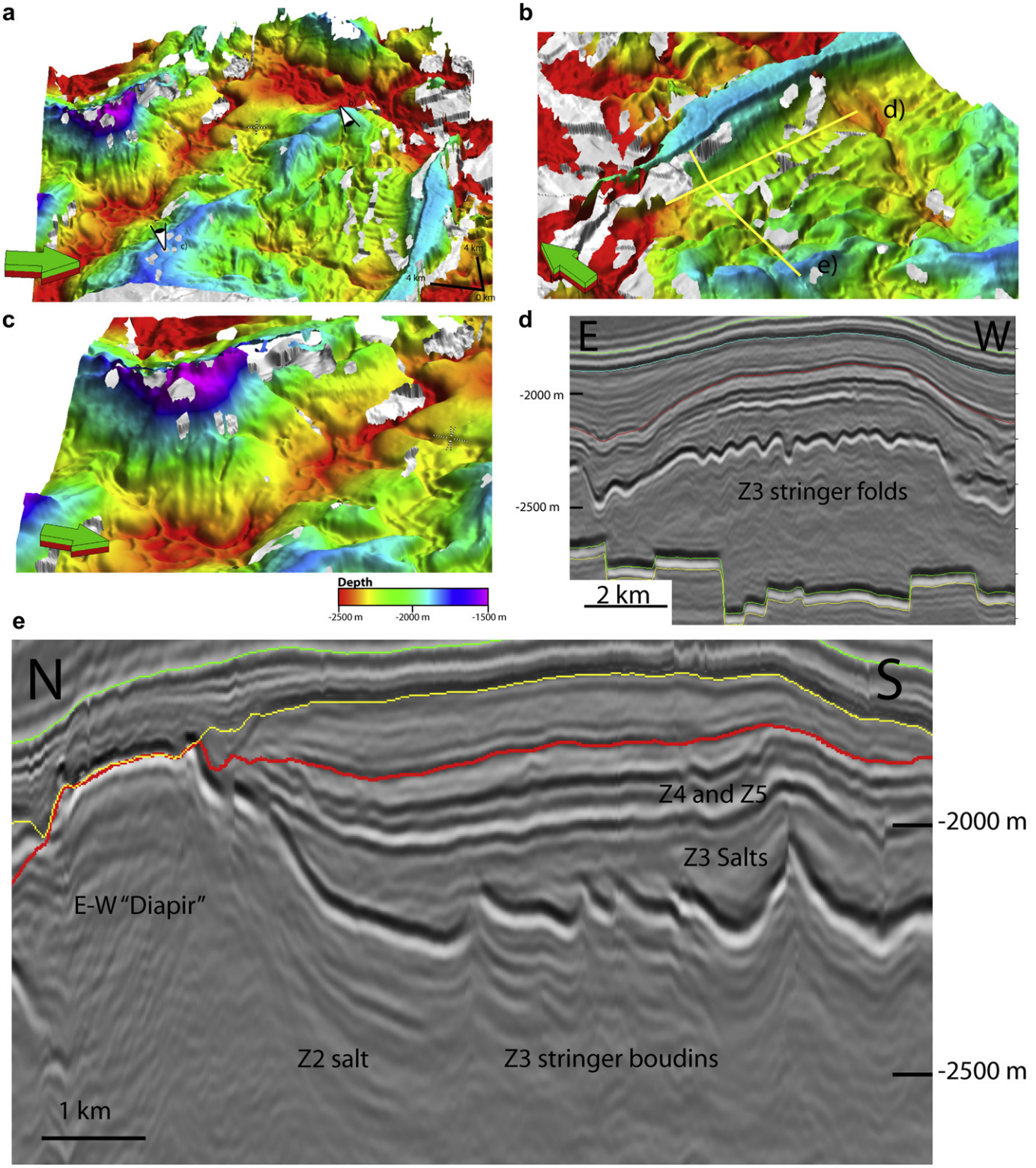

Fig. 6. Observations of folds and boudins in the Groningen area. (a) Oblique view of the top stringer horizon with zones thinner than 5 m made transparent to show top basement (grey) below. View directions of (b) and (c) are indicated in (a). (b) Oblique view of the constriction folds south of the EW diapir. Note how the TZ crossing the diapir influence the orientation of the holes in top stringer. Width of image is about 10 km (c) View of constriction folds on the flank of a salt structure in the south of the study area. Also note the slightly raised centre of the TZ in the valley at the base of the pillow. Width of image is about 8 km. (d) Cross-section perpendicular to the fold axes, location shown in yellow in (b) showing open folds (note vertical exaggeration). Also note the TZ in the most Western part of the cross-section. (e) Cross-section parallel to the fold axes, location shown in yellow in (b), cutting the diapir. The profile shows a series of broken, asymmetric monoclines with wavelengths between 250 and 1000 m. See discussion for interpretation of these structures. (For interpretation of the references to colour in this figure legend, the reader is referred to the web version of this article.)

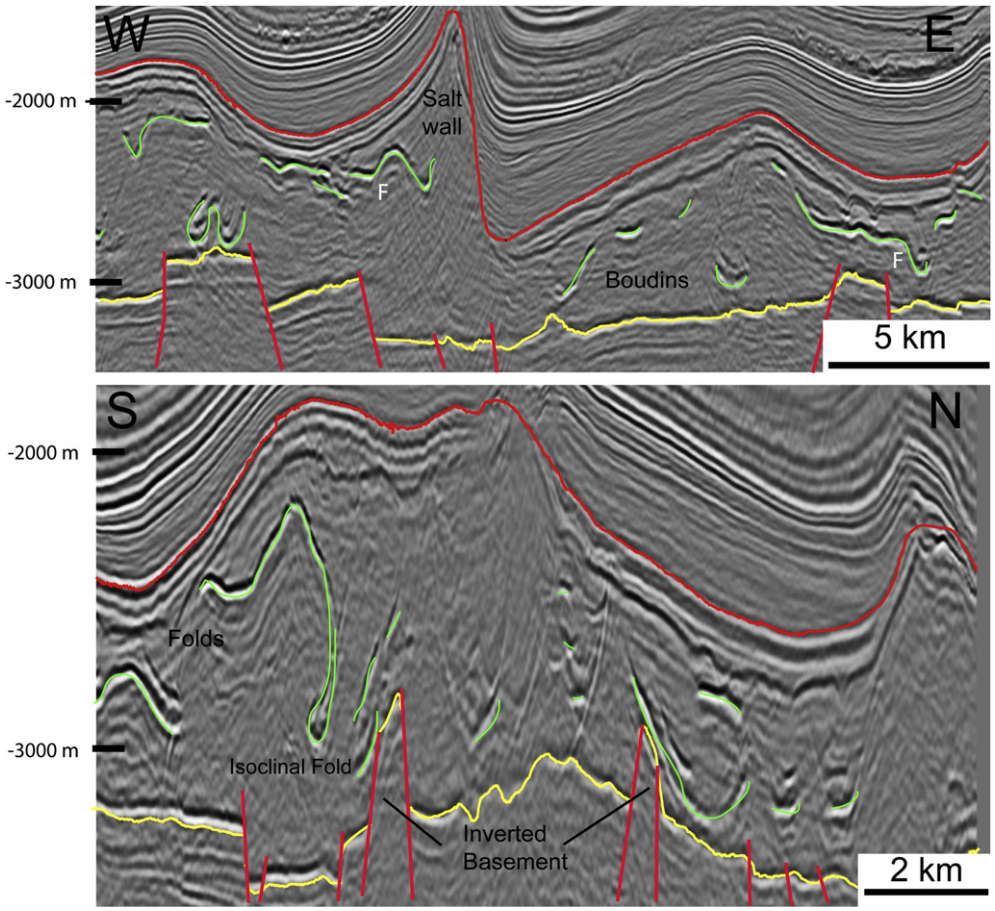

Fig. 7. Cross-sections through the Western Offshore area. For locations see Fig. 8d. Note that the boudins (see discussion) and the isoclinally folded stringers are located close to the inverted basement blocks. The isoclinal fold in the N–S cross-section is also shown in Fig. 11a and d.

the tip of the steep zone, but also up to 1000 m vertically, offsetting the stringer across almost the whole Zechstein. In map view, these discontinuities have a peculiar, curved morphology (Fig. 8f) with no clearly defined preferred orientation. In the point cloud some of these offsets resemble ductile ruptures (Fig. 11c). Fold axes are often at right angles to these offsets.

4.2.2. Areas with no visible stringer in the Western Offshore

Stringers are usually not visible in the steeply dipping discontinuities described above (see Figs. 10 and 12). However, in relatively flat-lying parts the stringers are also frequently not visible. Some of these ANVIS can be shown to be related to the basement structures (Fig. 8) or to structures in the overburden (Fig. 9). Other ANVIS like those in the east of the survey (Fig. 8c and d) are parallel to the salt wall.

4.2.3. Folds

The open folds (Figs. 7, 8 and 12) in the area have been described above. More striking are parts of the stringers which form complex, three dimensional, tight to isoclinally folded surfaces defined by the interpreted point cloud (Fig. 11). Visualization of these surfaces is difficult because of software limitations, and analysis of the structures was best done by interactively rotating the point cloud and defining the folded surfaces by visual inspection. In Fig. 11a, b and d some of these structural elements are shown as the raw point cloud together with a basic interpretation. It is striking that these structures have been only observed in direct proximity of inverted basement blocks.

Movies where the point clouds shown in Fig. 11 are rotated to get a better feel for the 3D structure are available on our website and YouTube Channel (www.ged.rwth-aachen.de and www.youtube.com/user/StrucGeology). Here also a direct comparison between the horizon and fault interpretation of the offshore study area can be found.

4.3. General description of observed fold types

Both in the Groningen area and offshore study area, folds are observed at different scales and with different morphologies. The structures can be classified in the following four different groups: (1) diapir-scale folds, (2) “constriction” folds, (3) strongly non-cylindrical structures and (4) isoclinal folds inside the salt structures. We will now discuss the interpretation of these in detail. We note here that our descriptions follow the “classical” fold description methods, focusing on 3D extrapolations of essentially 2D observations (Lisle and Toimil, 2007; Schmid et al., 2009). Defining the folded surfaces using differential geometry (Lisle and Toimil, 2007; Mynatt et al., 2007) will be used in a follow-up project.

4.3.1. Diapir-scale folds

At the regional scale of the salt structures the Z3 stringer resembles the top Zechstein surface (Figs. 3, 4, 7 and 8). This produces large, regional folds in the stringer’s enveloping surface which are harmonic with the large-scale salt structures and are therefore interpreted to reflect the large-scale flow paths during

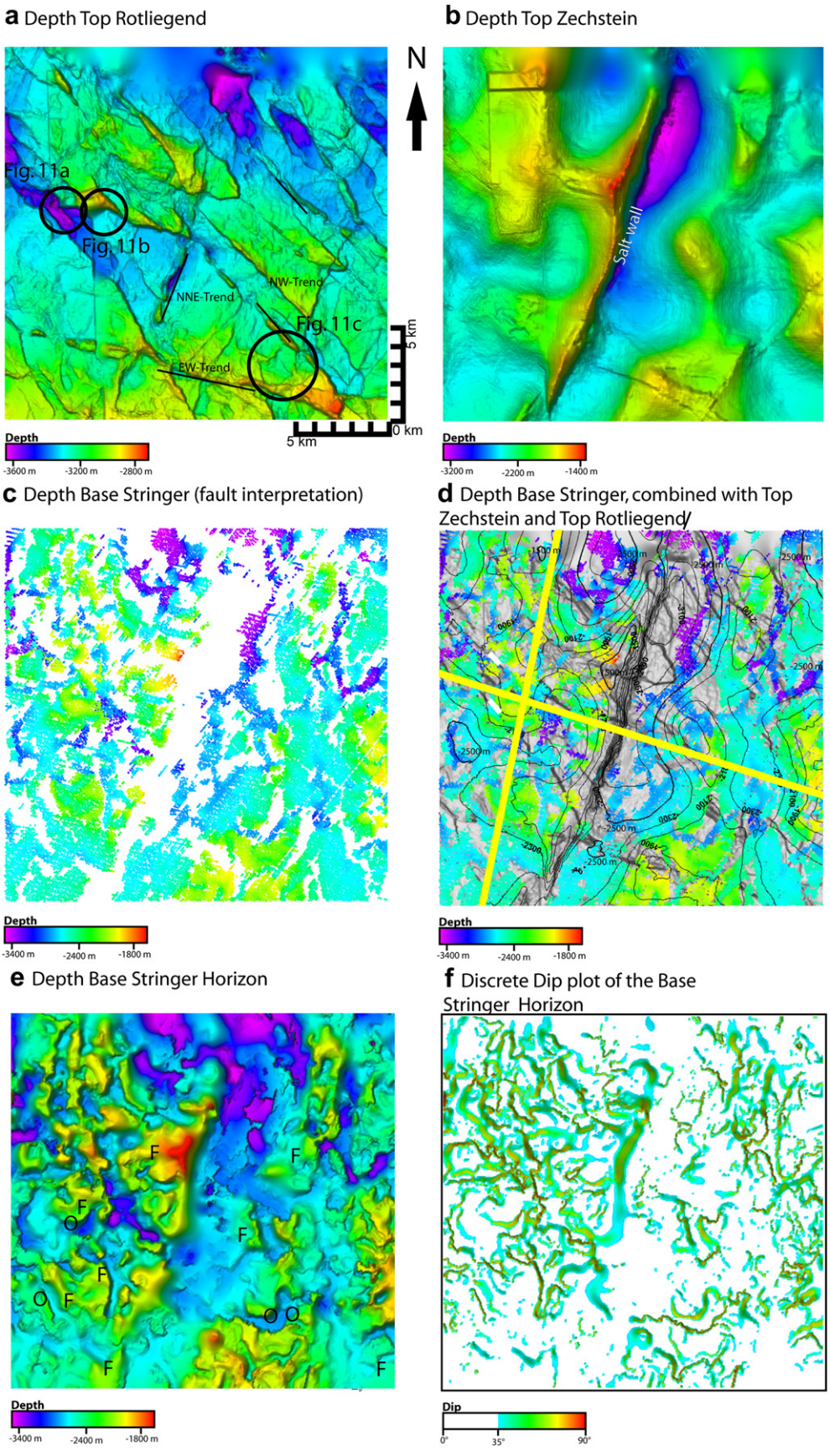
a Depth Top Rotliegend
N
Fig. 11a
Fig. 11b
Fig. 11c
NNE-Trend
NW-Trend
EW-Trend
5 km
0 km
5 km
Depth
-3600 m
-3200 m
-2800 m
b Depth Top Zechstein
Salt wall
Depth
-3200 m
-2200 m
-1400 m
c Depth Base Stringer (fault interpretation)
Depth
-3400 m
-2400 m
-1800 m
d Depth Base Stringer, combined with Top Zechstein and Top Rotliegend
Depth
-3400 m
-2400 m
-1800 m
e Depth Base Stringer Horizon
F
O
Depth
-3400 m
-2400 m
-1800 m
f Discrete Dip plot of the Base Stringer Horizon
Dip
0°
35°
90°

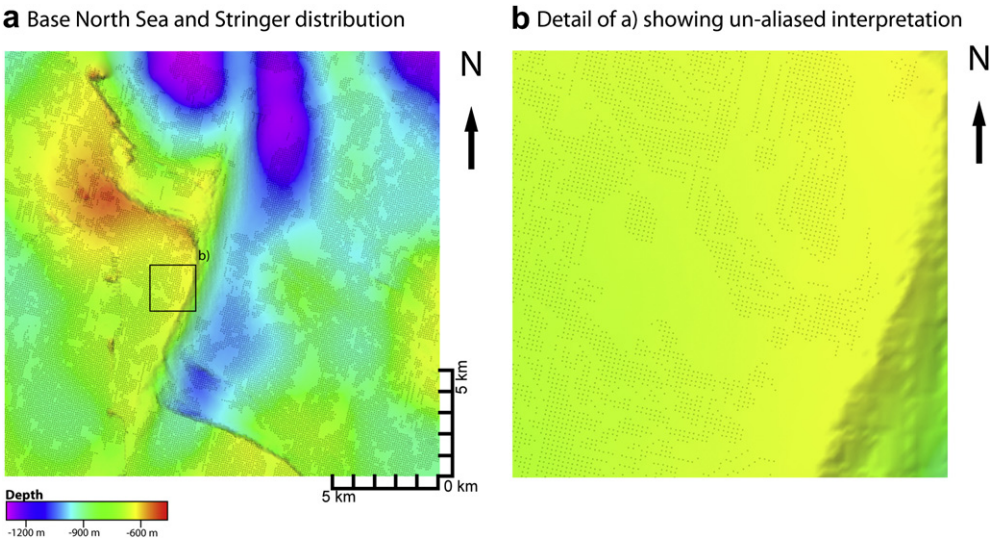

Fig. 9. Correlation between the stringer distribution and overburden structures. (a) Base North Sea Super Group (Base Cenozoic) reflector depth map, overlain by map showing where stringer interpretation is present (black points). Note the correlation between the NW–SE oriented structures in the depth map and the ANVIS in the stringer. (b) Detail of (a) showing interpretation of the stringer as individual points.

salt tectonics. The other three types of structures are disharmonic to this movement and interpreted to result from local deviations from the relatively simple deformation pattern expected (see Fig. 13a and d).

4.3.2. "Constriction" folds

When the fold axes are steeply dipping, folds in the Groningen area (Fig. 6) are interpreted as "constriction folds" similar to "curtain folds" (but the latter have vertical fold axes). These reflect simultaneous shortening and extension in the surrounding salt (cf. Zulauf and Zulauf, 2005, see also Fig. 13d) and implies that stringers underwent significant internal deformation and do not deform in a fully brittle fashion. Similar structures were described in many other studies in salt mines (see, for example: Lotze, 1957; Richter-Bernburg, 1980; Talbot and Jackson, 1987; Bornemann, 1991; Jackson et al., 1995) and in experiments (Escher and Kuenen, 1929; Jackson and Talbot, 1989; Koyi, 2001; Goscombe and Passchier, 2003; Goscombe et al., 2004; Zulauf and Zulauf, 2005; Chemia et al., 2008; Zulauf et al., 2009). Particularly the results of Callot et al. (2006) are very similar to the observed structure in Groningen directly south of the E–W diapir (here the pattern of holes in the stringer around the E–W diapir is similar to the pattern of ruptures in the analogue models, see also Fig. 13d). The open folds with sub-horizontal fold axes (Figs. 8e and 9) in the Western Offshore study area can also be interpreted to result from a constrictional process as the stringer moved along with the salt into the salt structure (see Fig. 13c).

4.3.3. Strongly non-cylindrical structures

Two types of non-cylindrical folds (see Pollard and Fletcher, 2005 for definitions) are observed. The first type is illustrated in Figs. 5 and 6a with a relatively large anticlinal stringer fold, harmonic to top salt, which is bisected by a TZ at high angle to the fold axis. The axial surface of this fold is (approximately) planar, but the fold hinge is lower where the TZ crosses this structure. We infer that TZ had a mechanical effect which influenced the buckling process and locally led to a longer wavelength, lower amplitude fold structure (Fig. 13b, Ramsay, 1967). Experimental and numerical modeling of the development of folds in layers with strongly variable initial thickness (Grujic, 1993; Grujic et al., 2002) is in agreement with this, but much more work is needed to allow a full interpretation.

The second type of non-cylindrical folds is observed in the offshore area. Here large areas of low amplitude folding with non-cylindrical axial planes, but relatively horizontal fold hinges (Fig. 13c, Pollard and Fletcher, 2005), are found (Figs. 8e and 9). These are very similar to structures formed in deformation of a constricted layer (Schmid et al., 2009) and constrictional plasticine experiments (Zulauf and Zulauf, 2005).

4.3.4. Isoclinal folds inside the salt structures

Although reliable interpretation of steeply dipping, complex structures is difficult, it is tempting to interpret tight to isoclinal folds in the stringers in a number of areas in the Western Offshore (Figs. 7 and 11). The structures shown in Fig. 11 closely resemble those documented in large salt structures by underground studies (cf. Krische, 1928; Richter-Bernburg, 1953a; Bornemann, 1991; Burliga, 1996; Behlau and Mingerzahn, 2001; Schléder et al., 2008) and experiments (Koyi, 2001; Callot et al., 2006; Chemia et al., 2008), and we propose that the high quality of our seismic data allows the 3D mapping of these structures in our study areas. These folds show strongly curved axial planes and fold axes and are associated with ruptures in the stringer (see below). In the regions where these structures dominate, deformation at the scale of the salt dome was clearly much more heterogeneous.

Fig. 8. Maps from the Western Offshore area. (a) Depth map top Rotliegend, note the different structural trends and the inverted blocks. (b) Depth map of top Zechstein. (c) Depth of the point cloud of the manually interpreted base stringer. (d) Same as (c) but overlaid on depth top Rotliegend surface and with contour lines of depth top Zechstein. (e) Depth of interpolated base stringer surface, based on autotracking plus interpolation interpretation. *F* denotes fold axes, *O* means vertical offsets, see also Fig. 12. (f) Only displaying the offset-parts of the autotracked and interpolated base stringer surface with a dip higher than 35°, marked *O* in (e). Sections are coloured for dip value. Note the extremely complex pattern of offsets. A movie of the comparison of the autotracked and manual interpretations of the stringer can be found on our website and YouTube Channel (www.ged.rwth-aachen.de and www.youtube.com/user/StrucGeology).

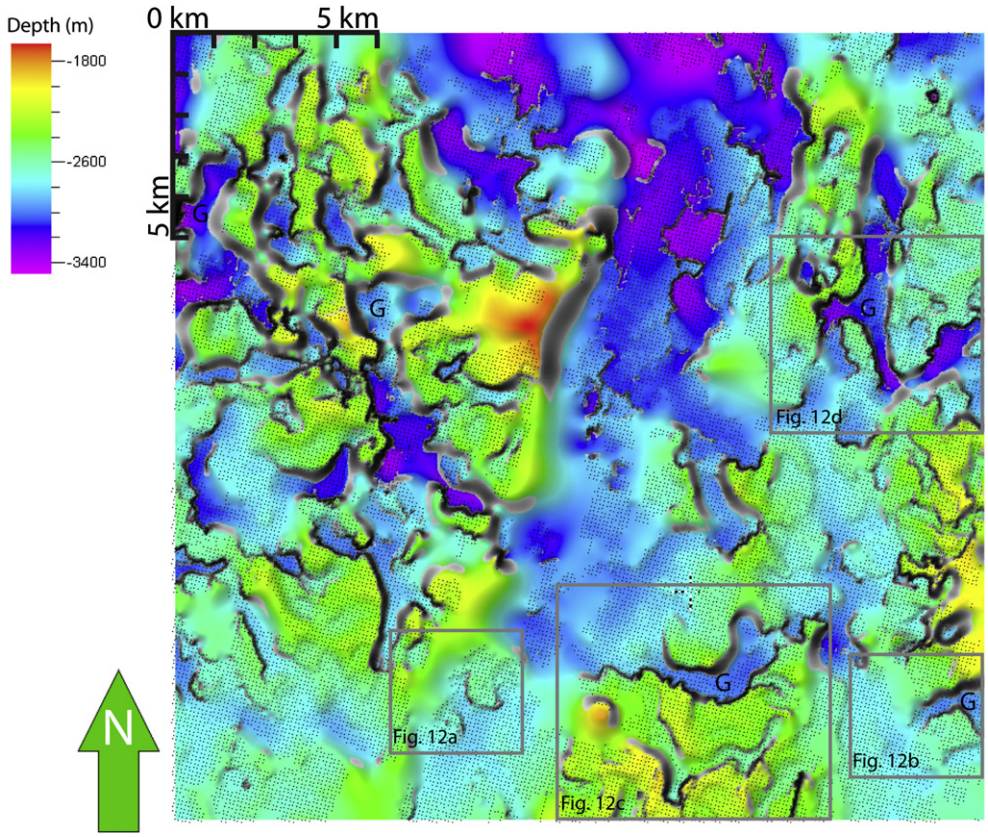

Fig. 10. Depth interpolated base stringer surface, based on autotracking and interpolation and the autotracked interpretation (as black points). Also shown are those areas where the dip of this surface is larger than 45° (ANVIS, grey, compare with Fig. 8e and f). ANVIS in areas where the surface is relatively flat-lying is shown by the absence of points in the coloured map. We interpret these ANVIS to represent boudin-necks in the stringer (see Fig. 10b). Also shown are several locations of the Graben-type offsets (G) and the locations of detailed views in Fig. 12.

5. Discussion

5.1. Interpretation of the thicker zones

The thickness of the Z3 stringer in the Groningen area and in the Western Offshore is generally about 40 m. Similar Z3 units are between 30 and 50 m thick in Poland, UK and Germany (Richter-Bernburg, 1980; Bornemann, 1991; Burliga, 1996; Smith, 1996). This shows that the thickness of the undisturbed Z3 stringer is relatively constant over large areas of the Zechstein basin, but local deviations are present like in the Blijham area (south of the Dollard Bay, Fig. 2) where the stringer is 80–90 m thick, perhaps related to the proximity of the Off-platform shoal (Fig. 2). Complex thickness variations are observed on the hydrocarbon field scale. Examples include the Vries area, south of Groningen (see Fig. 2 for location) and several other locations in the Netherlands (Rijks Geologische Dienst, 1991, 1993, 1995; TNO, 1998; Geluk, 2007; Geluk et al., 2007, this study).

Thickened zones (TZs) in this study were only observed in the Groningen study area and their increased thickness in seismic data is consistent with well data. They form a branching network (Figs. 4d–e and 5) of approximately in 4–5 km wide synclines (never anticlines), where the TZ is about 400 m wide and 300 m deeper than the surrounding stringer (Fig. 4f). In synclinal areas between salt pillows where the present-day top Zechstein is deep, TZs are more frequent than in areas where this horizon is shallow (Figs. 4f and 5). In cross-section at smaller scale, we observe internal overlapping reflectors and clear geometrical difference with respect to the surrounding thinner stringer (Fig. 5). In many cases, there is an ANVIS zone parallel to the TZ where the stringer is not visible.

The pattern of TZ and the peculiar internal structure cannot be explained by salt tectonics and basement-related faulting alone. In the following section we present one possible interpretation of the events leading to the development of the observed structures, other interpretations are certainly possible. We assert the formation of these structures to be the product of sedimentary and diagenetic processes, modified by deformation in the flowing salt. Keeping in mind the fact that the seawater during deposition of the Z3 stringer (clay, carbonate, anhydrite) is undersaturated with respect to the underlying Z2 halite, it is clear that any pathway for circulation of this seawater into the underlying Z2 halite will lead to strong dissolution, a system of karst caves and collapse structures which enhance further dissolution. Several authors describe sinkholes and collapse breccias related to karst in Z1 platform carbonates (Scholle et al., 1993; Southwood and Hill, 1995; Strohmenger et al., 1996). The early evolution of salt giants is still enigmatic (Hübscher et al., 2007), particularly with respect to karstification (Langbein, 1987). It is also possible that subtle (tectonic) movements during Zechstein times (Geluk, 2005) played a role in the development of the regional depressions and the incipient rupture of the Z3 clay, allowing solution of the Z2 evaporites.

Our preferred scenario involves the formation of 4–5 km wide depressions after deposition of the Grey Salt Clay (otherwise a thicker clay would later prevent groundwater circulation and formation of karst). In these depressions, during or after the deposition of the Z3 Anhydrite (but before the start of deposition of Z3 Halite from hypersaline brines), minor salt deformation led to the formation of an open fracture system in the Z3, allowing NaCl-undersaturated brines to circulate into the Z2 halite. This led to the

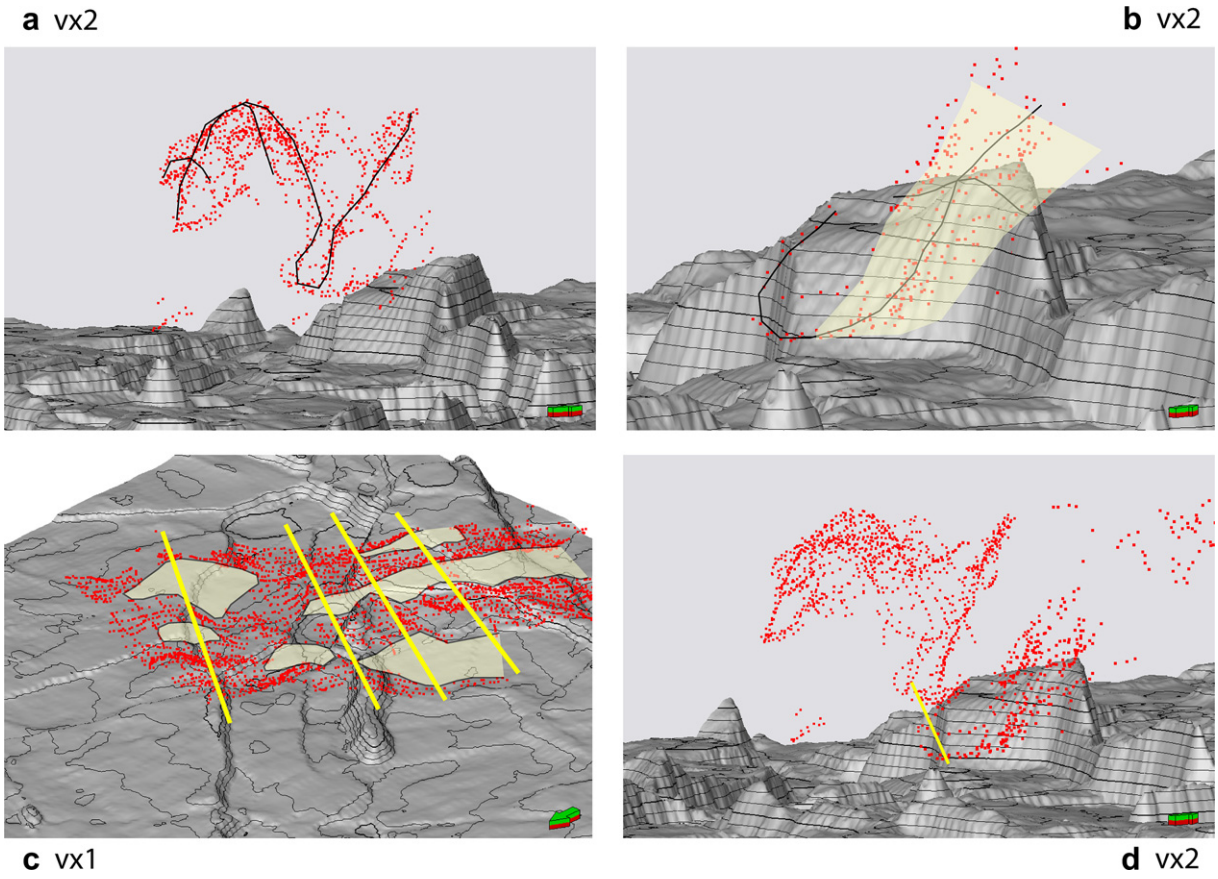

Fig. 11. Detailed observations of selections of the manual (point cloud) interpretation of the Z3 stringer in the Western Offshore study area. See Fig. 8 for locations. (a) Large-scale isoclinal fold, connected to a stringer with a dome-like shape. Black lines are manually drawn to illustrate the general shape. Note the proximity of this structure to the inverted basement (grey surface). Vertical exaggeration 2×. (b) Isoclinal fold close to inverted basement. Black lines and yellow surface indicate rough shape of the stringer. Vertical exaggeration 2×. (c) Detailed view of overlapping stringers in the Western Offshore area. Yellow planes are ANVIS, yellow lines are parallel to fold axes in this part of the stringer. No vertical exaggeration. (d) Combined point clouds of (a) and (b). Note how the fold hinges align (yellow line). Movies of the rotating point clouds of Fig. 11a–c can be found on our website and YouTube Channel (www.ged.rwth-aachen.de and www.youtube.com/user/StrucGeology). (For interpretation of the references to colour in this figure legend, the reader is referred to the web version of this article.)

formation of an extensive network of dissolution channels and collapse of overlying Z3. Sections of the Z3 stringer on the edges of the collapse zones ruptured and slid down the slope forming the ANVIS sub-parallel to TZ (Figs. 4 and 5). The slides collect at the base of the valleys resulting in the strongly deformed and tectonically thickened Z3 (TZ) observed in cross-sections (Fig. 5). In the Groningen area, the presence of what appears to be internal thrusts in seismic cross-sections and the presence of TZ in synclines rules out the interpretation that TZs are anhydrite diapirs, as these structures generally have a flat base (Fulda, 1928; Langbein, 1987; Williams-Stroud and Paul, 1997; Bäuerle et al., 2000). The observed structures are more compatible with early sliding structures (Richter-Bernburg, 1953b; Evrard et al., 2008).

The incursion of seawater into the Southern Permian Basin that is related to the deposition of the Z3 Stringer represents the most important Zechstein transgression and flooding of the Southern Permian Basin (Geluk, 2007). Little is known of the structures formed during the re-flooding of the centre of large salt basins, as most information is from the edge of the basins (Barber, 1981; Blanc, 2002; Rouchy and Caruso, 2002; Loget et al., 2005; Cornée et al., 2006). It is, however, easy to imagine currents (perhaps from the off-platform high; Fig. 2 and Bäuerle et al., 2000; Geluk, 2000) during Z3 carbonate deposition having formed erosional or karst structures when (halite-undersaturated) seawater was flowing over a halite substrate covered by a thin Grey Salt Clay layer. Sub-areal karst in salt forms the same structures as carbonate karst, but at faster rates (Bosá et al., 1999). In fact, the shape of the water-filled caves mapped by Bosá et al. (1999), including triple junctions, is remarkably similar to TZ in Groningen.

The formation of thicker zones in a deforming layer has significant implications for the evolution during salt tectonic deformation. Since the stringer is more competent than the surrounding host, the thicker zones of these layers represent stronger zones in this layer and will therefore be more difficult to deform. This will, for example, lead to different dominant wavelengths in folds (Ramsay, 1967; Grujic, 1993; Grujic et al., 2002). The thicker zones clearly influence the patterns of ANVIS and fold geometry in the study area (Figs. 5 and 13b).

5.2. Gravity-induced sinking

The density of natural halite is about 2200 kg/m^3, anhydrite is about 2900 kg/m^3, and dolomite is about 2850 kg/m^3 (Lide, 1995; Koyi, 2001; Chemia et al., 2008; Li et al., 2009). This density difference makes the stringers negatively buoyant and they tend to sink if the rheology of the surrounding salt allows this to happen at geologically significant rates.

The question of gravity-induced sinking of stringers has been a subject of much controversy (Gansser, 1992; Koyi, 2001; Callot et al., 2006; Chemia et al., 2008; Urai et al., 2008). Analogue and

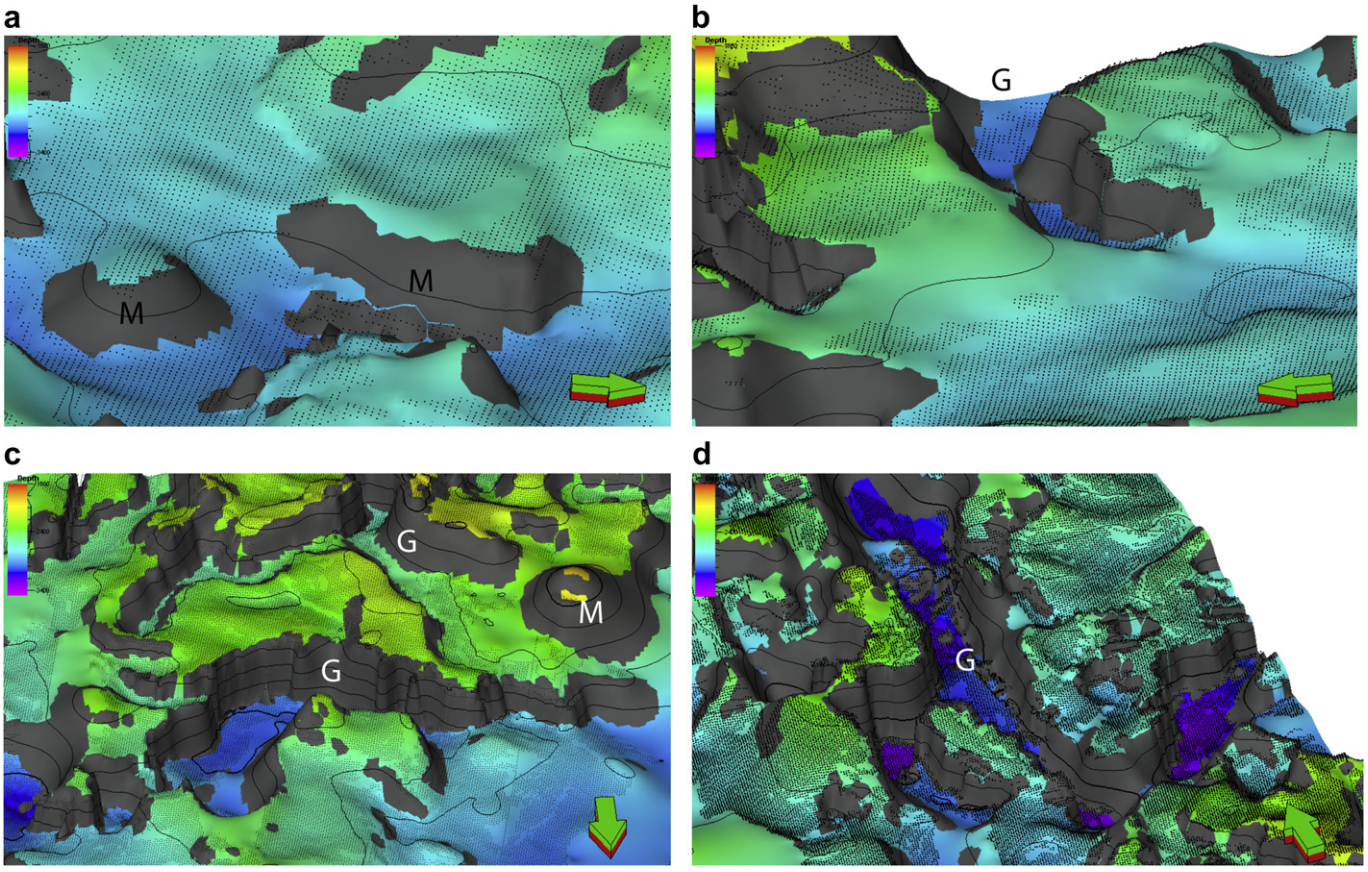

Fig. 12. Detailed observations of the autotracked base stringer interpretation (points), overlain on the interpolated surface (as in Figs. 8e and 9). Those sections of this surface that dip steeper than 45° are grey in colour. Locations of detailed views are shown in Fig. 9. Indicated are monocline-like offsets (M) in (a) and (c) and graben-like offsets (G) in (b) and (d). Note the differences in ANVIS where the stringer is quite flat (no points on coloured surface), like in (a) and (b) and those steeper than 45° (no points where the surface is grey). Note the curved shape of all ANVIS in map view. The vertical exaggeration is 2×. (For interpretation of the references to colour in this figure legend, the reader is referred to the web version of this article.)

numerical models show that dense blocks in diapirs sink when the diapiric-rise velocity is not sufficiently high to keep the blocks in the diapir (Koyi, 2001; Callot et al., 2006; Chemia et al., 2008). However, estimates of the in situ rheology of salt vary widely (cf. Urai et al., 2008), and consequently there is much uncertainty about the expected in situ sinking rates. It would therefore be useful to obtain additional constraints based on our results on this process. Diagnostic structures which allow separating salt tectonics-related and gravitational sinking-related processes are difficult to define but could consist of a correlation between vertical position of the stringer and stringer size (Li et al., 2009). Such a correlation is not apparent in our dataset. Keeping in mind that the major salt tectonic movements occurred before the end of the Cretaceous, the fact that many of our stringers are located high in the Zechstein (about 250 m from top Zechstein) can be used to calculate an upper bound of sinking velocity. Considering the case that these stringers were first ruptured into individual bodies, tectonically displaced to top Zechstein and then started to sink 65 Ma, the upper bound velocity is around 4 m/Myr. This is much lower than the rates suggested by some analogue and numerical models and is in agreement with the wide variation of salt rheologies used by the different studies, calling for more work to resolve this question.

5.3. Folding

In salt mines (see, for example, Krische, 1928; Richter-Bernburg, 1953a; Lotze, 1957; Talbot and Jackson, 1987; Schléder, 2006; Schléder et al., 2007) isoclinal folds are common even in apparently flat-lying salt. The folded layers are often associated with boudins (Ramsay and Huber, 1987; Schléder, 2006). High strain, folded intervals are often located close to less strongly deformed salt. This indicates that flow in evaporites can be strongly partitioned, possibly associated with the strong topography of the inverted basement blocks (compare with: Talbot and Jackson, 1987). Also the presence of shear zones in salt can add to the complexity (Kupfer, 1976; Schléder, 2006).

5.4. Interpretation of ANVIS

There are four possible explanations for the absence of a stringer in seismic sections. First, it may not have been deposited in this location. Second, the layer may be too thin to be imaged. Third, it may be discontinuous after being disrupted by tectonic deformation. Fourth, it may be in an orientation, which is too steep to produce a seismic reflection (Sleep, 1995; Geluk et al., 2000). The first explanation is rejected considering regionally constant thickness of the Z3. The well data from the Groningen area which were available for this study (see above) do not allow a clear distinction between alternatives two, three and four. However, it is not possible to explain all ANVIS by steep orientation only, because they also occur in areas where the surrounding stringer is shallow-dipping and has no vertical offset.

Keeping in mind that a full explanation of ANVIS in the Zechstein requires additional data from many wells and that in some

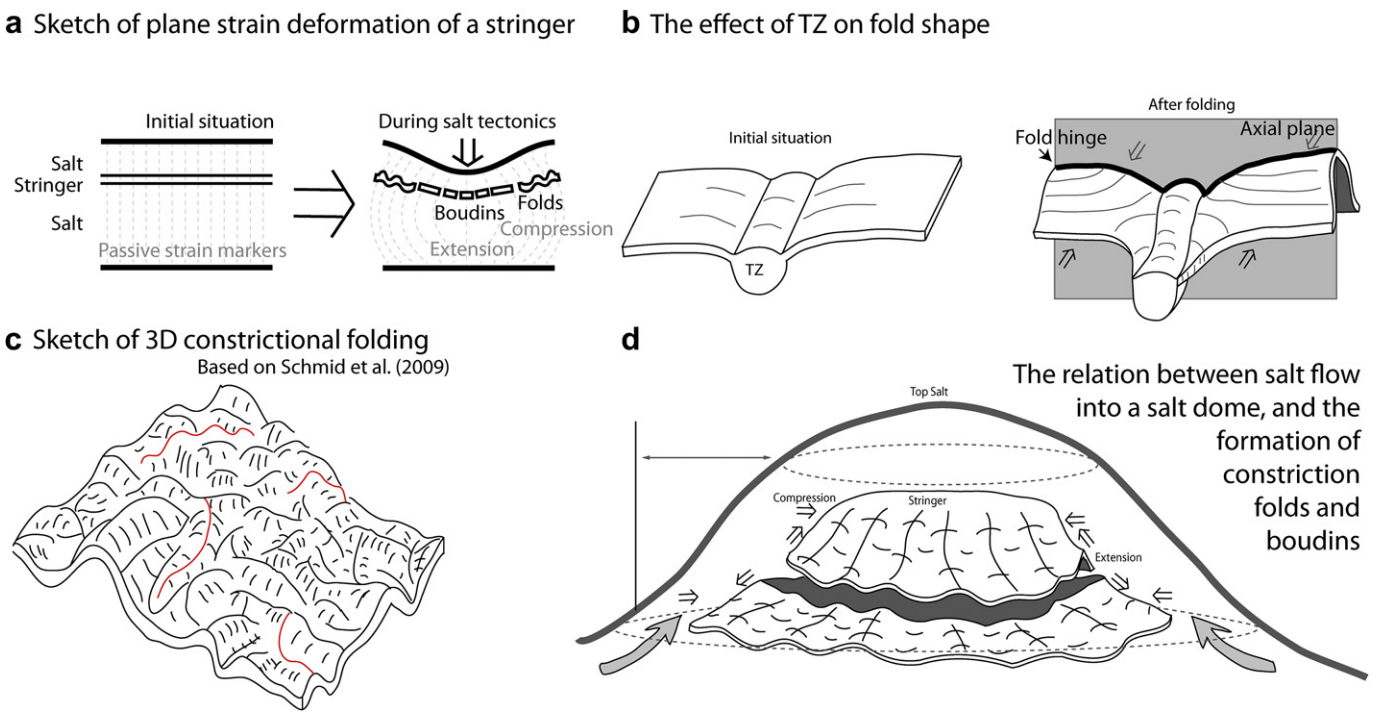

Fig. 13. Sketches of the structures observed in this study. (a) First-order, plane-strain structural evolution in a salt pillow, showing areas of layer-parallel extension and shortening and the corresponding boudinage in areas of top salt subsidence and folding in the salt pillows. Note that the shape of the stringer should resemble top Zechstein as a harmonic fold. (b) The effect of a thicker zone perpendicular to the folding is a depressed fold hinge while the axial plane is roughly planar. The TZ is stronger and this influences the shape of the fold. (c) In a constrictionally folded layer, the resulting fold structures have non-cylindrical axial planes. This is a different kind of "non-cylindrical folds" as those described in (b). (d) The formation of constriction folds and concentric boudins due to flow into a salt dome (compare with the concentric boudins in Figs. 4d and 6). The combined effect of the tensile forces due to vertical extension and coeval horizontal compression due to the decrease in salt dome diameter results in the contemporary formation of contradicting structural styles.

ANVIS steeply dipping stringers were found by drilling, in what follows, we make the reasonable assumption that in areas where the stringers' enveloping surface dips less than 30°, ANVIS correspond to the absence of a stringer due to tectonic disruption (boudinage). In areas where the stringers' enveloping surface dips more than 30°, ANVIS can either correspond to the absence of a stringer due to tectonic disruption (boudinage or faulting) or to a tectonically tilted stringer which is not imaged seismically.

5.5. Boudinage in salt – observations in mines

We interpret some of the fracturing of the stringer in the data to result from boudinage. The best examples of boudinage in our study areas are shown in Figs. 4d, 6b and e, 7, 8c and 11c, but the data quality does not allow a detailed description. We will compare our results with published example of boudinage in this section. The process of boudinage is the "disruption of layers, bodies or foliation planes within a rock mass in response to bulk extension along the enveloping surface" (Goscombe et al., 2004), and a boudin can be described as "a fractured sheet of rock situated between non-fractured (…) rocks" (Lohest, 1909; Ramberg, 1955; see also Sintubin, 2008).

There is large variety of boudin geometries which can be subdivided both according to their kinematics as well as to the shape of the boudin blocks (see Goscombe and Passchier, 2003; Goscombe et al., 2004). Boudinage of brittle inclusions in salt is described by several authors. Lotze (1957, p. 294; Smith, 1996; Davison, 1996; Roth, 1953; Borchert and Muir, 1964; Siemeister, 1969; Burliga, 1996; Schléder, 2006; Schléder et al., 2007; 2008). The six published wells of the Gorleben salt structure (Bornemann, 1991) penetrate the Z3 stringer for a total of eight times in four wells. In three of these penetrations the stringer is interpreted to be disrupted, faulted or fractured, showing the high fracture density in the Z3 stringer.

5.5.1. Boudinage in 3D

Studies of boudins to date have almost exclusively been in 2D profiles, and although there is a reasonable understanding of the range of structures occurring in profile view, there is a striking lack of understanding of the 3D morphology of boudins.

A 3D exposure of pegmatite boudins in marble (Schenk et al., 2007) shows boudins that are bound by a set of normal faults formed by reactivation of Mode-I fractures. The most extensive study to date of how boudins evolve in 3D is provided by the model experiments of Zulauf and coworkers (Zulauf et al., 2003, 2009; Zulauf and Zulauf, 2005). These experiments employ plasticine and natural anhydrite as strong layers. Here the plasticine is sufficiently ductile to fold when shortened parallel to the layering but at the same time sufficiently brittle to rupture if extended parallel to the layers, much like natural anhydrite. The patterns of this "ductile rupture" are much more complicated than brittle fracture patterns. It is clear that the deviation from plane-strain deformation results in the formation of very complex structures.

5.5.2. Boudin dimensions

Since the thickness of the stringer in Groningen (Figs. 3 and 6e) is between 40 and 50 m, the observed boudins have unusually high aspect ratios, in the order of 5–20, much larger than the largest mean aspect ratios described by Goscombe et al. (2004) in siliciclastic and carbonate rocks. In the Kłodawa salt mine, aspect ratios of around 20 are observed in the larger boudins (Burliga, 1996). The exceptional torn halite boudins in a carnallite matrix (Borchert and Muir, 1964; Siemeister, 1969) have aspect ratios in the order of 2.5–5 (assuming the view is perpendicular to the extension

direction) and also the experimental D1-boudins of Zulauf and Zulauf (2005) have aspect ratios around 5. Observations of boudins of sand in viscous putty (Callot et al., 2006) also indicate a high aspect ratio. On the other hand, Zulauf et al. (2009) produced experimental boudins of very brittle anhydrite in halite with aspect ratios of 1.5 ± 1.0. This difference in aspect ratio between the boudins of Goscombe et al. (2004) and "evaporitic" boudins may originate from the different rheologies, but more work is needed to resolve this question.

5.6. The rheology of salt and anhydrite during salt tectonic deformation

The rheology of anhydrite at shallow depth in the crust is not well known (Urai et al., 2008). We note that during shortening, anhydrite layers in salt domes commonly form concentric folds (see above), which means that the viscosity ratio is rather high, but at the same time boudins (brittle structures) are formed in extension. Corresponding to the present state of research (Urai et al., 2008), our present preferred model is that rheology of anhydrite is controlled by pressure solution and is Newtonian in layer-parallel shortening. However, the high, near lithostatic, fluid pressures, commonly observed in stringers (Williamson et al., 1997), allow tensile failure in layer-parallel extension in the anhydrite encased in sealing salt. This model explains why the stringer forms ductile folds as well as brittle boudins at the same time. A similar model has already been proposed for pegmatites encased in marble (Schenk et al., 2007). Alternatively, brittle fracturing may be initiated in the underlying more brittle limestone and claystone (sensu Hansen et al., 2004).

Folds formed under plane strain can be used to approximate the relative viscosity of the two layers (Sherwin and Chapple 1968), using the Biot–Ramberg equations (Ramsay and Huber, 1987) for Newtonian fluids, or those of Smith (1977) for non-Newtonian fluids. It is tempting to apply a similar method here and to compare, for example, this normalized arc length of folds to the aspect ratio of boudins to calculate the relative viscosity. However, conventional folding theory is based on plane-strain deformation and this is not the case in our field area, so a simple analysis may lead to errors (Stefan Schmalholz, personal communication). In future work we will attempt to constrain the relative rheologies of halite and anhydrite by 3D numerical modeling (Schmid et al., 2009; Schmalholz and Podladchikov, 2001).

5.7. The early life of a salt giant

In summary, this study has shown early karst-related thickness variations overprinted by complex folding and boudinage, producing the complicated present-day geometry of the Z3 stringer. Possible effects of early karst, diagenesis or gravitational deformation, probably augmented by a local increase in sedimentation of the stringer, formed a network of ruptures and slide-related folds. This resulted in a series of thicker zones in the stringer. During the Early Mesozoic salt flow, the salt moved into the narrow stems of salt walls and diapirs (Fig. 13d). This resulted in the coeval folding and boudinage in the stringer, leading to significantly more complex structures than in plane strain. This complexity is further increased by the thicker zones which are significantly stronger than the surrounding stringer and might form preferred instabilities for folding and boudinage. When the growth of salt structures was halted, the possible sinking of the broken anhydrite blocks added even further complexity, although we do not expect this sinking to have geologically significant velocities.

A useful conceptual model for the displacement and deformation of stringers is that of passive and active processes. Passive means that the stringers are displaced by the flowing salt as passive objects and active means that the contrast in mechanical properties causes local instabilities, resulting in deformation, folding and boudinage of the stringers. It is also clear that the temporal evolution of the position or orientation of a stringer in a salt dome has a large effect on the strain history (Weijermars, 1988; Zulauf et al., 2003; Chemia et al., 2008).

An interesting observation of this study is the apparent consistent position of the TZ between salt pillows. This is surprising because the TZs are thought to be older than the main phase of salt tectonics and also much smaller than the first-order structures. If this correlation can be shown to be real by additional observations of the same correlation in different areas, it would point to a subtle feedback mechanism in which the early internal structure of the salt basin can have a large effect on the evolving structures. In previous work, the main drivers for this were thought to be deformation on basement faults, regional tilt of the basin and lateral differences in overburden stress (Hudec and Jackson, 2007) but not the internal structure. An interesting concept emerging from this project is then that active deformation of the stringers during the early life of the Zechstein salt giant can initiate feedback processes which control the evolution of the later instabilities and the growth of large-scale salt structures (Hübscher et al., 2007). One mechanism for this could be that weak early deformation of TZ affects the topography of the top of the salt, creating a small topography which controls sediment architecture and evolution of overburden load (cf Ings and Beaumont, 2010).

5.7.1. A toolbox to predict internal structure of salt bodies

The Zechstein of the Central European Basin has a fascinating, complexly folded structure which is known only in a few cases based on mining data. The methods outlined in this study can be used at a regional scale because the Z3 reflector is present almost everywhere and can be mapped in 3D using seismic reflection data which are available over very large areas (TNO-NITG, 2004).

Using the same 3D seismic data, the kinematics of the suprasalt sequence can be relatively accurately reconstructed using palinspastic reconstruction techniques (e.g. Mohr et al., 2005). Rheology of the Zechstein salt is not completely understood but is constrained by a large amount of data. It is clear that even relatively pure halite can have strain rates variable by two orders of magnitude at the same differential stress and temperature (Urai et al., 2008) making the mechanical structure of the Zechstein strongly layered.

This dataset can now be combined into geomechanical models starting from the reconstructed original structure of the Zechstein including stringers, with the palinspastically reconstructed kinematics of top salt as kinematic boundary conditions, and the final structure compared with the interpretation of the Z3 stringer from 3D seismic. In addition, differential stress can be measured by subgrain size piezometry in drill cores. This method therefore produces models which can be tested against observations and, if the test is passed, can predict the internal structure of the salt body in the whole volume.

6. Conclusions

1. We mapped complex internal structure of salt domes using 3D seismic reflection data. This opens the possibility to study the internal structure of the Zechstein and other salt giants in 3D using this technique, exposing a previously poorly known structure which is comparable in size and complexity to the internal parts of some orogens.

2. The evolutionary sequence of sedimentary and diagenetic processes, followed by deformation at different scales results in early thickness variations, overprinted by a range of fold and of boudin structures.
3. Flow heterogeneities in salt caused by presence of thickness variations in stringers are interpreted to lead to subtle topography of top salt, which in turn influenced sedimentation and deformation of overburden.
4. Our observations show no conclusive evidence for significant gravity-induced sinking of stringers.
5. The methods used in this study can be combined with numerical modeling to predict the internal structure of salt bodies without extensive drilling or construction of galleries.

Acknowledgements

JLU and MdK would like to express their gratitude to Paul Williams for his mentoring and many discussions on the geometry and kinematics of folding.

The authors thank the Nederlandse Aardolie Maatschappij (NAM, a Shell operated 50–50 joint venture with ExxonMobil) for providing the data. We gratefully acknowledge discussions with Peter Kukla and Stephan Back on stringer geology and seismic interpretation. This paper benefited considerably from discussion with Jos Terken, Joris Steenbrink and Daan den Hartog Jager (Shell). We also thank Mark Geluk for his discussion and comments.

Schlumberger is thanked for providing Petrel 2005 and 2007 seismic interpretation software under academic licence. The editor, Shoufa Lin, and the reviewers Gernold Zulauf and Charlotte Krawczyk are thanked for their comments which considerably improved the manuscript. Janneke IJmker is thanked for critical notes in the early stages of the MS.

References

Al-Siyabi, H.A., 2005. Exploration history of the Ara intrasalt carbonate stringers in the South Oman Salt Basin. GeoArabia 10 (4), 39–72.

Barber, P.M., 1981. Messinian subaerial erosion of the proto-Nile Delta. Marine Geology 44 (3–4), 253.

Bäuerle, G., Bornemann, O., Mauthe, F., Michalzik, D., 2000. Turbidite, Breccien und Kristallrasen am top des Hauptanhydrits (Zechstein 3) des Salzstocks Gorleben. Zeitschrift der Deutschen Geologischen Gesellschaft 151 (1–2), 99–125.

Behlau, J., Mingerzahn, G., 2001. Geological and tectonic investigations in the former Morsleben salt mine (Germany) as a basis for the safety assessment of a radioactive waste repository. Engineering Geology 61, 83–97.

Best, G., 1989. Die Grenze Zechstein/Buntsandstein in Nordwest-Deutschland nach Bohrlochmessungen. Zeitschrift der Deutschen Gesellschaft für Geowissenschaften 140, 73–85.

Blanc, P.L., 2002. The opening of the Plio-Quaternary Gibraltar Strait: assessing the size of a cataclysm. Geodinamica Acta 15, 303–317.

Borchert, H., Muir, R.O., 1964. Salt Deposits. The Origin, Metamorphism and Deformation of Evaporites. D. Van Nostrand Company, Ltd., London, New York, Toronto, p. 338.

Bornemann, O., 1991. Zur Geologie des Salzstocks Gorleben nach den Bohrergebnissen. BfS-Schriften 4, 1–67.

Bosá, P., Bruthans, J., Filippi, M., Svoboda, T., Šmíd, J., 1999. Karst and caves in salt diapirs, SE Zagros Mts (Iran). Acta Carsologica 28 (2), 41–75.

Burliga, S., 1996. Kinematics within the Klodawa salt diapir, central Poland. In: Alsop, G.I., Blundell, D.J., Davison, I. (Eds.), Salt Tectonics. Geological Society Special Publication 100. Geological Society, London, pp. 11–21.

Callot, J.-P., Rondon, D., Rigollet, C., Letouzey, J., Pillot, D., Mengus, J.-M., 2006. Stringers and evolution of salt diapirs, insight from analogue models. In: 2006 AAPG International Conference and Exhibition, Perth, Australia.

Chemia, Z., Koyi, H., Schmeling, H., 2008. Numerical modelling of rise and fall of a dense layer in salt diapirs. Geophysical Journal International 172, 798–816.

Coelewij, P.A.J., Haug, G.M.W., Kuijkv, H., 1978. Magnesium-salt exploration in the Northeastern Netherlands. Netherlands Journal of Geosciences/Geologie en Mijnbouw 57 (4), 487–502.

Cornée, J.J., Ferrandini, M., Saint Martin, J.P., Münch, P., Moullade, M., Ribaud-Laurenti, A., Roger, S., Saint Martin, S., Ferrandini, J., 2006. The late Messinian erosional surface and the subsequent reflooding in the Mediterranean: new insights from the Melilla-Nador basin (Morocco). Palaeogeography, Palaeoclimatology Palaeoecology 230 (1–2), 129.

Davison, I., 1996. Deformation and sedimentation around active Miocene salt diapirs on the Tihama Plain, Northwest Yemen. Geological Society Special Publications 100, 23.

De Jager, J., 2003. Inverted basins in the Netherlands, similarities and differences. Netherlands Journal of Geosciences/Geologie en Mijnbouw 82 (4), 355–366.

De Mulder, E.F.J., Geluk, M.C., Ritsema, I.L., Westerhoff, W.E., Wong, T.E., 2003. De ondergrond van Nederland. Wolters-Noordhoff, Groningen/Houten, p. 379.

Desbois, G., Zavada, P., Schléder, Z., Urai, J.L., 2010. Deformation and recrystallization mechanisms in actively extruding salt fountain: microstructural evidence for a switch in deformation mechanisms with increased availability of meteoric water and decreased grain size (Qum Kuh, central Iran). Journal of Structural Geology 32 (4), 580–594.

Duin, E.J.T., Doornenbal, J.C., Rijkers, R.H.B., Verbeek, J.W., Wong, T.E., 2006. Subsurface structure of the Netherlands – results of recent onshore and offshore mapping. Netherlands Journal of Geosciences/Geologie en Mijnbouw 85 (4), 245–276.

Escher, B.G., Kuenen, P.H., 1929. Experiments in connection with salt domes. Leidse Geologische Mededelingen 3, 151–182.

Evans, D.J., Chadwick, R.A. (Eds.), 2009. Underground Gas Storage: Worldwide Experiences and Future Development in the UK and Europe. Special Publications, Geological Society, London 313.

Evrard, E., Sellier, N., Vendeville, B.C., Loncke, L., Loubrieu, B., Brosolo, L., Mascle, J., 2008. Physical modelling of thin-skinned, salt-related gravitational deformation in response to active crustal-scale tectonics: examples from the eastern Mediterranean. In: Third International Geomodelling Conference, Florence, Italy, September 24, 2008, Bollettino di Geofisica, teorica ed applicate, Istituto Nazionale di Oceanografia e di Geofisica Sperimentale, 49, 366–371.

Fokker, P.A., Urai, J.L., Steeneken, P.V., 1995. Production-induced convergence of solution mined caverns in magnesium salts and associated subsidence. In: Proceedings of the Fifth International Symposium on Land Subsidence. The Hague/The Netherlands, A.A. Balkema, 281–289.

Fulda, E., 1928. Die Geologie der Kalisalzlagerstätten. In: Krische, P. (Ed.), Das Kali, II. Teil. Enke's Bbliothek für Chemie und Technik unter berücksichtiging der Volkswirtschaft 7. Ferdinand Enke, Stuttgart Germany, pp. 24–136.

Gansser, A., 1992. The enigma of the Persian dome inclusions. Eclogae Geologicae Helvetiae 85, 825–846.

Geluk, M.C., 1995. Stratigraphische Gliederung der Z2-(Staßfurt-) Salzfolge in den Niederlanden: Beschreibung und Anwendung bei der Interpretation von halokinetisch gestörten Sequenzen. Zeitschrift der deutschen Gesellschaft für Geowissenschaften 146, 458–465.

Geluk, M.C., 1997. Paleogeographic maps of Moscovian and Artinskian; contributions from the Netherlands. In: DSoleau, S., De Wever, P. (Eds.), Peri-thetys Stratigraphic Correlations, vol. 19. Geodiversitas, pp. 229–234.

Geluk, M.C., 2000. Late Permian (Zechstein) carbonate-facies maps, the Netherlands. Netherlands Journal of Geosciences/Geologie en Mijnbouw 79 (1), 17–27.

Geluk, M.C., 2005. Stratigraphy and Tectonics of Permo-Triassic Basins in the Netherlands and Surrounding Areas. Utrecht University.

Geluk, M.C., 2007. Permian. In: Wong, T.E., Batjes, D.A.J., De Jager, J. (Eds.), Geology of the Netherlands. Royal Netherlands Academy of Arts and Sciences, Amsterdam, pp. 63–84.

Geluk, M.C., Arts, R., Duin, E.J.T., Van Wees, J.-D., Oldenziel, C., Paar, W.A., 2000. The Zuidwending salt dome: a multidisciplinary mapping project. TNO-NITG – Information 5, 5–7.

Geluk, M.C., Paar, W.A., Fokker, P.A., 2007. Salt. In: Wong, T.E., Batjes, D.A.J., De Jager, J. (Eds.), Geology of the Netherlands. Royal Netherlands Academy of Arts ande Sciences, Amsterdam, pp. 283–294.

Goscombe, B.D., Passchier, C.W., Hand, M., 2004. Boudinage classification: end-member boudin types and modified boudin structures. Journal of Structural Geology 26, 739–763.

Goscombe, B.D., Passchier, C.W., 2003. Asymmetric boudins as shear sense indicators – an assessment from field data. Journal of Structural Geology 25 (4), 575–589.

Grujic, D., 1993. The influence of initial fold geometry on type 1 and type 2 interference patterns: an experimental approach. Journal of Structural Geology 15 (3–5), 293.

Grujic, D., Walter, T.R., Gärtner, H., 2002. Shape and structure of (analogue models of) refolded layers. Journal of Structural Geology 24 (8), 1313.

Hansen, D.M., Shimeld, J.W., Williamson, M.A., Lykke-Andersena, H., 2004. Development of a major polygonal fault system in Upper Cretaceous chalk and Cenozoic mudrocks of the Sable Subbasin, Canadian Atlantic margin. Marine and Petroleum Geology 21, 1205–1219.

Hofrichter, E., 1974. Speicherkavernen im Salzstoecken Nordwestdeutschlands -Geologische Probleme, Bemerkungen zur selektiven Aufloessing von Kalisalzen. Erzmetall 65 (5), 219–226.

Hübscher, C., Cartwright, J., Cypionka, H., De Lange, G., Robertson, A., Suc, J.P., Urai, J.L., 2007. Global look at salt giants. Eos 88 (16), 177–179.

Hudec, M.R., Jackson, M.P.A., 2007. Terra infirma: understanding salt tectonics. Earth Science Reviews 82 (1–2), 1–28.

Ings, S.J., Beaumont, C., 2010. Shortening viscous pressure ridges, a solution to the enigma of initiating salt 'withdrawal' minibasins. Geology 38, 339–342.

Jackson, M.P.A., 1985. Natural Strain in Diapiric and Glacial Rock Salt, with Emphasis on Oakwood Dome, East Texas. Bureau of Economic Geology/The University of Texas at Austin/Texas.

Jackson, M.P.A., 1995. Retrospective salt tectonics. In: Jackson, M.P.A., Roberts, D.G., Snelson, S. (Eds.), Salt Tectonics: a Global Perspective, 65. AAPG Memoir, pp. 1–28.

Jackson, M.P.A., Cornelius, R.R., Craig, C.H., Gansser, A., Stocklin, J., Talbot, C.J., 1990. Salt Diapirs of the Great Kavir, Central Iran. Geological Society of America, Boulder. Memoir 177,p. 139+ Karte.
Jackson, M.P.A., Roberts, D.G., Snelson, S. (Eds.), 1995, Salt Tectonics - A Global Perspective. AAPG Memoir, 65. AAPG, Tulsa, U.S.A, p. 454. Bulletin.
Jackson, M.P.A., Talbot, C.J., 1989. Anatomy of mushroom-shaped diapirs. Journal of Structural Geology 11 (1/2), 211–230.
Jackson, M.P.A., Vendeville, B.C., 1994. Regional extension as a geologic trigger for diapirism. Geological Society of America Bulletin 106, 57–73.
Koyi, H., 2001. Modeling the influence of sinking anhydrite blocks on salt diapirs targeted for hazardous waste disposal. Geology 29 (5), 387–390.
Krische, P. (Ed.), 1928, Das Kali (parts I and II). Enke's Bibliothek für Chemie und Technik unter berücksichtiging der Volkswirtschaft, 7. Ferdinand Enke, Stuttgart, Germany, p. 768.
Kupfer, D.H., 1968. Relationship of internal to external structure of salt domes. Diapirism and diapirs: a symposium. Memoir – American Association of Petroleum Geologists 8, 78–89.
Kupfer, D.H., 1976. Shear zones inside Gulf Coast salt stocks help to delineate spines of movement. AAPG Bulletin 60 (9), 1434–1447.
Langbein, R., 1987. The Zechstein sulphates: the state of the art. In: Peryt, T.M. (Ed.), The Zechstein Facies in Europe. Lecture Notes in Earth Sciences. Springer, Berlin/ Heidelberg, pp. 143–188.
Li, S., Abe, S., Urai, J.L., Van Gent, H.W., 2009. Sinking of Carbonate and Anhydrite Stringers in Rock Salt: Insights from Numerical Simulations. In: EGU General Assembly 2009, Vienna, Austria, 19–24 April 2009, Geophysical Research Abstracts, 11.
Lide, D.R. (Ed.), 1995. CRC Handbook of Chemistry and Physics. A Ready Reference Book of Chemical and Physical Data. CRC Press, Boca Raton, New York, London, Tokyo.
Lisle, R.J., Toimil, N.C., 2007. Defining folds on three-dimensional surfaces. Geology 35, 519–522.
Loget, N., Van Den Driessche, J., Davy, P., 2005. How did the Messinian salinity crisis end? Terra Nova, 414–419.
Lohest, M., 1909. De l'origine des vienes et des géodes des terrains primaires de Belgique. Annales de la Societe Geologique de Belgique 36B, 275–282.
Lotze, F., 1957. Steinsalz und Kalisalze, 1. Teil (Allgemein-geologischer Teil), 1. Gebruder Borntraeger, Berlin, pp. 465.
Mattes, B.W., Conway Morris, S., 1990. Carbonate/evaporite deposition in the late Precambrian-Early Cambrian Ara formation of southern Oman. In: Robertson, A.H.F., Searle, M.P., Ries, A.C. (Eds.), The Geology and Tectonics of the Oman Region. Geological Society (London) Special Publication 49, pp. 617–636.
Maystrenko, Y., Bayer, U., Scheck-Wenderoth, M., 2006. 3D reconstruction of salt movements within the deepest post-Permian structure of the Central European Basin System – the Glueckstadt Graben. Netherlands Journal of Geosciences/ Geologie en Mijnbouw 85 (3), 181–196.
Mohr, M., Kukla, P.A., Urai, J.L., Bresser, G., 2005. Multiphase salt tectonic evolution in NW Germany: seismic interpretation and retro-deformation. International Journal of Earth Sciences (Geologische Rundschau) 94, 914–940.
Van der Molen, A.S., 2004. Sedimentary Development, Seismic Stratigraphy and Burial Compaction of the Chalk Group in the Netherlands North Sea Area. PhD. thesis, UtrechtUniversity.
Muehlberger, W.R., 1968. Internal structures and mode of uplift of Texas and Louisiana salt domes. Saline Deposits 88. Geological Society of America Special Papers, 359–364.
Mynatt, I., Bergbauer, S., Pollard, D.D., 2007. Using differential geometry to describe 3-D folds. Journal of Structural Geology 29, 1256–1266.
Peters, J.M., Filbrandt, J.B., Grotzinger, J.P., Newall, M.J., Shuster, M.W., Al-Siyabi, H.A., 2003. Surface-piercing salt domes of interior North Oman, and their significance for the Ara carbonate "stringer" hydrocarbon play. GeoArabia 8 (2), 231–270.
Pollard, D.D., Fletcher, R.C., 2005. Fundamentals of Structural Geology. Cambridge University Press, Cambridge. 500pp.
Ramberg, H., 1955. Natural and experimental boudinage and pinch-and-swell structures. Journal of Geology 63, 512–526.
Ramsay, J.G. (Ed.), 1967. Folding and Fracturing of Rocks. McGraw-Hill Book Company, New York, San Francisco, St. Louis, Toronto, London, Sydney, p. 568.
Ramsay, J.G., Huber, M.I., 1987. Folds and Fractures, the Techniques of Modern Structural Geology, 2. Academic Press, London.
Remmelts, G., 1996. Salt tectonics in the southern North Sea, the Netherlands. In: Rondeel, H.E., Batjes, D.A.J., Nieuwenhuijs, W.H. (Eds.), Geology of Gas and Oil under the Netherlands. Kluwer Academic Publishers, Dordrecht, pp. 19–30.
Reuning, L., Schoenherr, J., Heimann, A., Urai, J.L., Littke, R., Kukla, P.A., Rawahi, Z., 2009. Constraints on the diagenesis, stratigraphy and internal dynamics of the surface-piercing salt domes in the Ghaba salt basin (Oman): a comparison to the Ara group in the South Oman Salt Basin. GeoArabia 14 (3), 83–120.
Richter-Bernburg, G. (Ed.), 1953a. Salzlagerstätten (Proceedings of the Frühjahrstagung der Deutschen Geologische Gesellschaft, Goslar, May 13–16, 1953). Zeitschrift der Deutschen Geologischen Gesellschaft, 105, pp. 589–908.
Richter-Bernburg, G., 1953b. Stratigraphische Gliederung des deutschen Zechsteins. Zeitschrift der Deutschen Geologischen Gesellschaft 105, 593–645.
Richter-Bernburg, G., 1980. Salt tectonics, interior structures of salt bodies. Bulletin des centre de recherches exploration-production Elf-Aquitain 4 (1), 373–393.
Richter-Bernburg, G., 1987. Deformation within salt bodies. In: Lerche, I., O'Brien, J.J. (Eds.), Dynamical Geology of Salt and Related Structures. Academic Press, Inc., pp. 39–75.
Rijks Geologische Dienst (RGD), 1991. Map Sheet II Ameland–Leeuwarden, Explanation to Map Sheet II Ameland–Leeuwarden. Rijks Geologische Dienst (RGD), Haarlem, the Netherlands. 87.
Rijks Geologische Dienst (RGD), 1993. Map Sheet V Sneek-Zwolle, Explanation to Map Sheet V Sneek-Zwolle. Rijks Geologische Dienst (RGD), Haarlem, the Netherlands. 126.
Rijks Geologische Dienst (RGD), 1995. Map Sheet III Rottumeroog–Groningen, Explanation to Map Sheet III Rottumeroog–Groningen. Rijks Geologische Dienst (RGD), Haarlem, the Netherlands. 113.
Roth, H., 1953. Ausbildung und Lagerungsformedn des Kalifözes "Hessen" im Fuldagebiet. Zeitschrift der Deutschen Geologischen Gesellschaft 105, 674–684.
Rouchy, J.M., Caruso, A., 2002. Review: the Messinian salinity crisis in the Mediterranean basin: a reassessment of the data and an integrated scenario. Sedimentary Geology 188–189, 35–67.
Scheck, M., Bayer, U., Lewerenz, B., 2003. Salt redistribution during extension and inversion inferred from 3D backstripping. Tectonophysics 373, 55–73.
Schenk, O., Urai, J.L., Van der Zee, W., 2007. Evolution of boudins under progressively decreasing pore pressure – a case study of pegmatites enclosed in marble deforming at high grade metamorphic conditions, Naxos, Greece. American Journal of Science 307, 1009–1033.
Schléder, Z., 2006. Deformation Mechanisms of Naturally Deformed Rocksalt. PhD thesis, Rheinisch-Westfälischen Technischen Hochschule aachen.
Schléder, Z., Burliga, S., Urai, J.L., 2007. Dynamic and static recrystallization-related microstructures in halite samples from the Kłodawa salt wall (central Poland) as revealed by gamma-irradiation. Neues Jahrbuch für Mineralogie und Petrologie 184 (1), 17–28.
Schléder, Z., Urai, J.L., Nollet, S., Hilgers, C., 2008. Solution-precipitation creep and fluid flow in halite: a case study of Zechstein (Z1) rocksalt from Neuhof salt mine (Germany). International Journal of Earth Sciences 97 (5), 1045–1056.
Schmalholz, S.M., Podladchikov, Y.Y., 2001. Strain and competence contrast estimation from fold shape. Tectonophysics 340, 195–213.
Schmid, D.W., Dabroski, M., Krotkiewski, M., 2009. Structure of fold traps. Physics of hydrocarbon bearing systems. In: The 22nd Kongsberg Seminar, Kongsberg, Norway, 6–8 May.
Schoenherr, J., Reuning, L., Kukla, P.A., Littke, R., Urai, J.L., Siemann, M., Rawahi, Z., 2009a. Halite cementation and carbonate diagenesis of intra-salt reservoirs from the Late Neoproterozoic to Early Cambrian Ara group (South Oman Salt Basin). Sedimentology 56 (2), 567–589.
Schoenherr, J., Schléder, Z., Urai, J.L., Littke, R., Kukla, P.A., 2009b. Deformation mechanisms of deeply buried and surface-piercing Late Pre-Cambrian to Early Cambrian Ara salt from interior Oman. International Journal of Earth Sciences. doi:10.1007/s00531-009-0443-3 online first.
Scholle, P.A., Stemmerik, L., Ulmer-Scholle, D., Di Liegro, G., Henk, F.H., 1993. Palaeokarst-influenced depositional and diagenetic patterns in Upper Permian carbonates and evaporites, Karstryggen area, central East Greenland. Sedimentology 40, 895–918.
Schultz-Ela, D.D., Walsh, P., 2002. Modeling of grabens extending above evaporites in Canyonlands National Park, Utah. Journal of Structural Geology 24 (2), 247–275.
Schwerdtner, W.M., Van Kranendonk, M., 1984. Structure of Stolz diapir; a well-exposed salt dome on Axel Heiberg Island, Canadian Arctic Archipelago. Bulletin of Canadian Petroleum Geology 32 (2), 237–241.
Sherwin, J.-A., Chapple, W.M., 1968. Wavelengths of single layer folds. A comparison between theory and observation. American Journal of Science 266, 167–178.
Siemann, M.G., Ellendorff, B., 2001. The composition of gases in fluid inclusions of late Permian (Zechstein) marine evaporites in Northern Germany. Chemical Geology 173, 31–44.
Siemeister, G., 1969. Primärparagenese und Metamorphose des Ronnenbergslagers nach Unterschuchungen im Grubenfeld Salzdetfurth, 62. Bundesanstalt für Bodenforschung und den Geologischen Landesämtern der Bundesrepublik Deutschland, Hannover, pp. 122.
Sintubin, M., 2008. Photograph of the month: boudin centennial. Journal of Structural Geology 30, 1315–1316.
Sleep, N.H., 1995. Ductile creep, compaction, and rate and state dependent friction within major fault zones. Journal of Geophysical Research 100 (B7) 13,065–13,080.
Sleep, N.H., Fujita, K., 1997. Principles of Geophysics. Blackwell Science, USA.
Smith, R.B., 1977. Formation of folds, boudinage, and mullions in non-Newtonian materials. Geological Society of America Bulletin 88, 312–320.
Smith, D.B., 1995. Chapter 3: north-east England (Durham Province), marine Permian of England. Geological Conservation Review 8, 205.
Smith, D.B., 1996. Deformation in the late Permian Boulby halite (EZ3Na) in Teesside, NE England. Geological Society Special Publications 100, 77–88.
Southwood, D.A., Hill, W.O.R., 1995. The origin and distribution of porosity in the Zechstein Kalk (Upper Permian) of Hewett field, southern north sea. Petroleum Geoscience 1, 289–302.
Stäuble, A.J., Milius, G., 1970. Geology of Groningen gas field, Netherlands. Geology of Giant Petroleum Fields AAPG A009, 359–369.
Strohmenger, C., Voigt, E., Zimdars, J., 1996. Sequence stratigraphy and cyclic development of Basal Zechstein carbonate–evaporite deposits with emphasis on Zechstein 2 off-platform carbonates (Upper Permian, Northeast Germany). Sedimentary Geology 102 (1–2), 33.

Talbot, C.J., 2008. Photograph of the month. Journal of Structural Geology 30 (7), 810.
Talbot, C.J., Aftabi, P., 2004. Geology and models of salt extrusion at Qum Kuh, central Iran. Journal of the Geological Society 161, 321–334.
Talbot, C.J., Jackson, M.P.A., 1987. Internal kinematics of salt diapirs. AAPG Bulletin 71 (9), 1068–1093.
Taylor, J.C.M., 1998. Upper Permian–Zechstein. In: Glennie, K.W. (Ed.), Petroleum Geology of the North Sea. Basic Concepts and Recent Advances, fourth ed. Blackwell Science, Oxford, pp. 174–211.
TNO, 1998. Map Sheet X Almelo-Winterswijk, Geological Atlas of the Subsurface of the Netherlands. Netherlands Institute for Applied Geoscience TNO – National Geological Survey Haarlem, 142.
TNO-NITG, 2004. Geological Atlas of the Subsurface of the Netherlands – Onshore. TNO-NITG, Utrecht, p. 103.
Urai, J.L., Schléder, Z., Spiers, C.J., Kukla, P.A., 2008. Flow and transport properties of salt rocks. In: Littke, R., Bayer, U., Gajewski, D., Nelskamp, S. (Eds.), Dynamics of Complex Intracontinental Basins: The Central European Basin System. Springer-Verlag, Berlin, Heidelberg, pp. 277–290.
Van Adrichem-Boogaert, H.A., Kouwe, W.F.P., 1993–1997. Stratigraphic nomenclature of the Netherlands; revision and update by RGD and NOGEPA. TNO-NITG, Mededelingen Rijks Geologische Dienst. Haarlem 50, 50.
Van Eijs, R., Breunse, J., 2003. Evidence for two different creep mechanisms in rocksalt – solution mining in the Barradeel concession. TNO-NITG – Information, 5–9.
Van Gent, H.W., Back, S., Urai, J.L., Kukla, P.A., Reicherter, K., 2009. Paleostresses of the Groningen area, the Netherlands – results of a seismic based structural reconstruction. Tectonophysics – Progress in Understanding Sedimentary Basins 470 (1–2), 147–161.
Van Hoorn, B., 1987. Structural evolution, timing and tectonic style of the Sole Pit inversion. In: (Editor). P.A.Z. (Ed.), Compressional Intra-plate Deformations in the Alpine Foreland. Tectonophysics 137, 239–284.
Van Keken, P.E., Spiers, C.J., Van den Berg, A.P., Muyzert, E.J., 1993. The effective viscosity of rocksalt: implementation of steady-state creep laws in numerical models of salt diapirism. Tectonophysics 225 (4), 457–476.
Warren, J.K., 2006. Evaporites: Sediments, Resources and Hydrocarbons. Springer, p. 1035.
Weijermars, R., 1988. Convection experiments in high Prandtl number silicones, Part 2. Deformation, displacement and mixing in the Earth's mantle. Tectonophysics 154 (1–2), 97.
Wijhe, Van, D.H., 1987. Structural evolution of inverted basins in the Dutch offshore, Compressional Intra-plate Deformations in the Alpine Foreland. Tectonophysics 137, 171–219.
Williams-Stroud, S.C., Paul, J., 1997. Initiation and growth of gypsum piercement structures in the Zechstein basin. Journal of Structural Geology 19 (7), 897.
Williamson, M.A., Murray, S.J., Hamilton, T.A., Copland, M.A., 1997. A review of Zechstein drilling issues. SPE Drilling and Completion 13 (3), 174–181.
Wong, T.E., Batjes, D.A.J., de Jager, J. (Eds.), 2007. Geology of the Netherlands. Edita-KNAW, Amsterdam, p. 354.
Ziegler, P.A., 1982. Geological Atlas of Western and Central Europe. Elsevier Scientific Publishing Company, The Hague, Amsterdam, p. 130.
Zirngast, M. (Ed.), 1991. Die Entwicklungsgeschichte des Salzstocks Gorleben, Ergebnis einer strukturgeologischen Bearbeitung. Geologisches Jahrbuch. Reihe A: Allgemeine und Regionale Geologie BR Deutschland und Nachbargebiete, Tektonik, Stratigraphie, Palaeontologie, Heft 132. Herausgegeben von der Bundesanstalt für Bodenforschung und den Geologischen Landesämtern der Bundesrepublik Deutschland, Hannover, p. 31.
Zirngast, M., 1996. The development of the Gorleben salt dome (northwest Germany) based on quantitative analysis of peripheral sinks. In: Alsop, G.I., Blundell, D.J., Davison, I. (Eds.), Salt Tectonics, 100. Geological Society Special Publications, pp. 203–226.
Zulauf, G., Zulauf, J., Hastreiter, P., Tomandl, B., 2003. A deformation apparatus for three-dimensional coaxial deformation and its application to rheologically stratified analogue material. Journal of Structural Geology 25, 469–480.
Zulauf, G., Zulauf, J., Bornemann, O., Kihm, N., Peinl, M., Zanella, F., 2009. Experimental deformation of a single-layer anhydrite in halite matrix under bulk constriction. Part 1: geometric and kinematic aspects. Journal of Structural Geology 31 (4), 460.
Zulauf, J., Zulauf, G., 2005. Coeval folding and boudinage in four dimensions. Journal of Structural Geology 27, 1061–1068.